, STUDY OF PHOTOCONDUCTIVITY IN UNDOPED TELLURIUM

bу

N.G. Shyamprasad, B. Tech. (I.I.T., Madras)

A thesis submitted to the Faculty of Graduate Studies and Research in partial fulfillment of the requirements for the degree of Master of Engineering

Department of Electrical Engineering

McGill University

Montreal, Canada

August, 1979

ABSTRACT

Preliminary photoconductivity studies were made on tellurium Bulk single crystal samples and thin film polycrystalline samples. The dependence of photoconductive sensitivity on sample thickness and openation was specifically studied. The spectral distribution of photoconductive sensitivity was obtained at 77 K.

The results indicate that the sensitivity is not dependent on sample orientation although a clear dependence on polarisation direction was seen. The sensitivity for bulk single crystals increases with decreasing thickness, whereas for the thin film polycrystalline samples there is a decrease with decreasing thickness. An optimum thickness of about 100 microns is predicted for a maximum photoconductive sensitivity.

The surface recombination velocities were calculated from the spectral dependence of photoconductivity. Absorption coefficients were also calculated in the range 1.5 to 4 microns. A very rough estimate of D^{\pm} has been calculated to be 2×108 cmHz $\frac{1}{2}$ watt $^{-1}$ at 23 Hz.

RESUMÉ

Des études préliminaires de la photoconductivité furent effectuées sur des échantillons monocristaux d'une masse de tellurium et sur des échantillons d'une mince couche polycristalline. La dépendance de la sensibilité photoconductrice selon l'épaisseur et l'orientation de la masse furent spécialement étudiées. La distribution spéctrale de la sensibilité photoconductrice fut obtenue à 7.7 K.

Les résultats indiquent que la sensibilité ne dépend pas l'orientation de la masse bien qu'on ait constate une nette dépendance sur la direction de la polarisation. La sensibilité pour les masses monocrystallines augmante à mesure que leur épaisseur diminué, alors quelle diminue dans les même condition pour les échantillons d'une mince couche polycrystalline. Une épaisseur optimale d'environ 100 micromètres est prédite avec une sensibilité maximale.

Les vitesses de recombinaison de la surface furent calculées à partir de la dépendance spectrale de la photoconductivité. Les coefficients d'absorption furent aussi calculées dans un ordre de 1.5 à 4 micromètres. Un estimé très primaire du D* fut calculé à $2x10^8$ cmHz $^{\frac{1}{2}}$ watt $^{-1}$ à 23 Hz.

ACKNOWLEDGEMENTS

The author wishes to place on record his sincere gratitude to Dr. C.H. CHAMPNESS for his constant guidance, encouragement and assistance in every possible aspect of this study.

The assistance of Dr. M.C. Jain in fabricating the thin film samples is very much appreciated.

Thanks are due to Dr. E.J. Fjarlie of RCA Research Laboratories, St. Anne de Bellevue, Que. for his assistance in conducting detectivity measurements.

Acknowledgements are due to the Selenium-Tellurium Development Association Inc. for the partial financial support of this work.

TABLE OF CONTENTS

,		,	Page
ABSTRAC	r '		. 1
RESUME	• • • • • • •)	. ii
ACKNOWLI	e dg em en,t	s	. 111
TABLE O	F CONTEN	тѕ .,	. iv
CHAPTER	ľ	INTRODUCTION	. 1
CHAPTER	II	THEORY OF PHOTOCONDUCTIVITY	. 7
	2.1	Qualitative Description	. 7
	2.2	Simplified Treatment	
	2.3	More Exact Treatment	
CHAPTER	III	TELLURIUM SAMPLE PREPARATION	. 18
•	3.1	Bulk Samples	18
	3.1a	Slicing and surface polishing	
*	3.1b	Sample cutting	. 19
,	3.1c	Mounting into holder	. 20
	3.2	Thin Film Samples	. 20
	3.2a	Substrate preparation	. 21
	3.2b	Electrode deposition	. 21
	3.2c	Tellurium deposition	. 22
•	3.2d	Au-Te-Au structure	. 23
CHAPTER	ıy	MEASUREMENT TECHNIQUES AND APPARATUS	. 33
	4.1	Monochromatic Illumination Source	. 33
•	4.1a	Source unit	
	4.1b	Monochromator unit	. 33
	4.1c	Internal detector and amplifier	. 34
æ	4.2	External Apparatus	. 34
	4.2a	Optics	. 34
	4.2b	Cryostat	. 35
	4.2c	Measuring circuit	. 35
	4.3	Calibration of the Thermocouple Detecto	r 36
	<i>l. l.</i>	The bear and up blad by Manager and	

																																,		
CHAPTER	V .		PH	01	:0	CC	N	DU	JC	T	[V	Ί	T	ľ	R	E	S	UI	T	S	•	•	•	•	•	• •	•	•	•	• •	• •	•	46	•
	5.1		ь Ви	11		Sa	1 12D	n 1	ľe	8			•			•	٠,		٠.						•					•			46	ó
	5.1																																47	
	51																																48	
	5.1	- 20																															48	
	5.1																																48	
	5.2																																49	
	J • 4		# 11		L	F		ш	3	a :	# P	_	6	9	•	•	•	• •	•	•	• •	•	•	•	•	• •	•	æ.	•	•	•	•	7.	
CHAPTER	VI		IN	TI	R	PΕ	RE	T	ÌΤ	I	O N	ī	01	F	R	E	S	UI	T	S	•	•	•	•	•	• •	• •	•	•	•		•	61	l
•	6.1		Th	10	: k	ne	2 S	8	D	e	pe	e n	d	e r	ıc	e		• •		•	• •				•	• •		•		•		•	61	l
	6.2	(Su	rí	a	C	•	Re	e C	01	n b	1	n	a t	: 1	0	n	1	ē o	r	i	3 u	1	k	;	Sé	ķ	p	i	e	ş	•	62	2
	6.3		Ab	8	r	рſ	i	οr	1	C	0 6	e f	f	10	: 1	. e	n	t	•	•	• •	•	•	•	•	• (• •	•	•	•	• •	•	64	4
CHAPTER	VII		DI	S	วบ	s	SI	01	ı	A	N E)	C	ON	1 C	L	U	S	0	N	S	•	•	•	•	•	• •	•	•	•		•	75	5
	7.1		Di	. 6 (2 u	8 1	، 1 ع	01	n.				•	• •	•	•		<u>,</u>			• •			•	•				•	•		•	7 5	5
•	7.2		Su	m	a	ry	7	o f	E	C	01	ıc	1	u e	1	0	n	s		•	• •		•	•	•			•	•			•	79	3
	7.3																																80	
REFEREN	CES	• • •	 • • •	•	• •	•	۷, • •	•		•	•	•	•	•		•	•	•	• •	•	•	• •	•	•,	•	•	٠.	. 4	•	•			8	1
APPENDI	(A	• • •	 	•							• •										•			•	•					•			8:	3

CHAPTER I

1)

INTRODUCTION:

The elemental semiconductor tellurium exists as an optically uniaxial positive crystal, which exhibits birefringence, dichroism and optical activity. As has been discussed elsewhere, the trigonal crystal structure of tellurium consists of helical chains, each helix having three atoms per turn. The electronic band structure has been studied widely and the prime concern as regards the photoconductivity is the existence of a direct energy gap of approximately 0.32 eV between the valence and the conduction bands.

The study of photoconductivity in semiconductors has been and still is a topic of great interest for many reasons. It leads to a better understanding of band structure and of recombination and trapping mechanisms. In addition, there are, many applications for the effect, particularly as a detector of infrared radiation. Although early infrared detectors were made with polycrystalline films, the developments in crystal growing and material purification techniques have ushered in a new era for such devices. Semiconductors for common detectors include extrinsic materials such as germanium, doped with gold (2 to 10 microns), with copper (3 to 20 microns) and with mercury (3 to 12 microns) on the one hand. On the other hand, there

are intrinsic materials such as pure germanium (1 to 1.7 microns), indium antimonide (1.5 to 5 microns), lead sulfide (0.7 to 2.5 microns) and mercury-cadmium-telluride (6 to 12 microns).

The performance of tellurium as a detector has been stated² to rival that of PbS, which is a very commonly used detector material. However, there has been insufficient experimental work done on tellurium to verify its merit as a photoconductive detector, due partly to non-availability of good single crystals and uncertain sample preparation techniques. Apart from its possible device potential, there is a need for a better characterisation of photoconductivity in tellurium, especially in crystals with a minimum of imperfections, since this material is known to be very susceptible to lattice damage. This was the motivation for the present work. Further, the availability of high quality crystals grown in our laboratory³ by the Czochralski method acted as a catalyst for such a study.

Specifically the dependence of photoconductive sensitivity on a) wavelength of irradiation, b) crystallographic
orientation of the sample and c) thickness of the sample was
measured at 77 K. In all cases undoped tellurium samples
were used. This study is of a preliminary nature and as such
limited in scope. More detailed cresearch is needed to
complete the characterisation. For example a serious attempt
to carry out noise measurements for evaluating tellurium as
a photodetector was not done.

Review of Past Work on Tellurium

The spectral distribution of photoconductivity in evaporated tellurium films was studied by Moss⁴ in 1949. These films were deposited on graphite electrodes on the inner walls of small Pyrex dewar flasks and had thicknesses of the order of 1 micron. The peak of the spectral distribution was found to be around 1.3 microns with the samples cooled to 90 K.

Photoconductivity studies in bulk single crystal tellurium were made by Loferski⁵ in 1953, although his main objective was to measure the optical absorption coefficient. The crystals for his photoconductivity measurements were grown by the Bridgman method and his samples were etched in nitric acid. He reported two peaks in the spectral distribution of photoconductivity at 3.24 and 3.72 microns with the magnitude of the former peak varying with polarisation of the E-vector with respect to the c-axis.

Edwards and Mercado² calculated the theoretical limits of performance of tellurium as a photoconductive detector, limited by background radiation noise, and the predicted Noise Equivalent Power (NEP) was 5.1x10⁻¹³ watts. They reported an even smaller measured value of 3.1x10⁻¹³ watts, but did not elaborate on this result.

Vis⁶ studied the steady-state and transient photoconductive behaviour in tellurium single crystals. His samples were obtained by cleaving the crystal at liquid nitrogen temperature, shaping into units with side arms by a jet of abrasive particles, etching in a chromic-hydrochloric

acid solution and finally giving a treatment in hot concentrated sulfuric acid. He found a response time of 350.

µsec for T<77 K, which decreased with increase of the intensity of radiation. These results were explained in terms of a trapping model.

A detailed study of photoconductivity in tellurium was carried out by Grosse and Winzer?. They used undoped bulk single crystal tellurium samples of different thicknesses; cut abrasively and subsequently etched. They measured the spectral dependence at 77 K and the photoconductive decay to determine the lifetime of excess carriers. In their analysis, which is used in this thesis, they calculated the recombination velocities to be in the range 545 to 1300 cm/sec for the (1010) surface and 2800 to 3500 cm/sec for the (0001) plane. They also noticed polarisation dependent oscillations in the photoconductive sensitivity, which were attributed to the presence of a damaged surface layer.

Thesis Structure

The structure of the present thesis is as follows:

The theory of photoconductivity in a semiconductor is presented in Chapter II for an infinitely long sample, which is considered adequate for the analysis of the experimental results. The method of preparation of the samples, both in monocrystalline bulk form and polycrystalline thin film form, is described in Chapter II. This is followed by a description of the apparatus and measurement techniques in Chapter IV. The results of photoconductivity measurements

.

are presented in Chapter V' and analyzed in respect to surface recombination velocity and absorption coefficient in Chapter VI. The results of the study are discussed finally in Chapter VII. For the convenience of the reader a list of terms commonly used in photoconduction work is collected together in Table I.

TABLE I

Photoconductivity Figures of Merit

(Watt cm^{-2})

NEI NEI =
$$\frac{J_e N}{V}$$
 Noise Equivalent Input (Watt cm⁻²)

NEP = JeNA Noise Equivalent Power (Watt)

Jones' S S =
$$\frac{P_n}{A} \left(\frac{f}{\Delta f}\right)$$
 Jones' Sensitivity (Watt cm⁻¹)

D*
$$D^* = \frac{A (\Delta f)}{P_n}$$
 Normalized Detectivity
$$(cmHz watt^{-1})$$

$$S_1 = \frac{V}{J_e V_b} \frac{(R_p + R_s)^2}{4R_p R_s}$$
 Specific Sensitivity (cm watt⁻¹)

 $J_e = rms$ value of energy flux (watt cm⁻²)

V - rms value of signal voltage as measured (volt)

N .= rms noise voltage (volt)

, A = area of the cell (cm^2)

7

 $P_n = noise$ equivalent power (watt)

f = modulating frequency (Hz)

Af = frequency bandwidth (Hz)

R_D = dark resistance of detector (ohm)

Rg = logd resistance (ohm)

 v_b = bias voltage applied across the detector and resistor (volt)

CHAPTER II

THEORY OF PHOTOCONDUCTIVITY

2.1 Qualitative Description of Photoconductivity

Photoconductivity is the process by which the electrical conductivity of a material is changed by incident electromagnetic radiation. Absorption of some of the incident energy causes an excess generation of current carriers, over and above the thermal equilibrium level. Due to this addition of carriers, an enhanced conduction occurs.

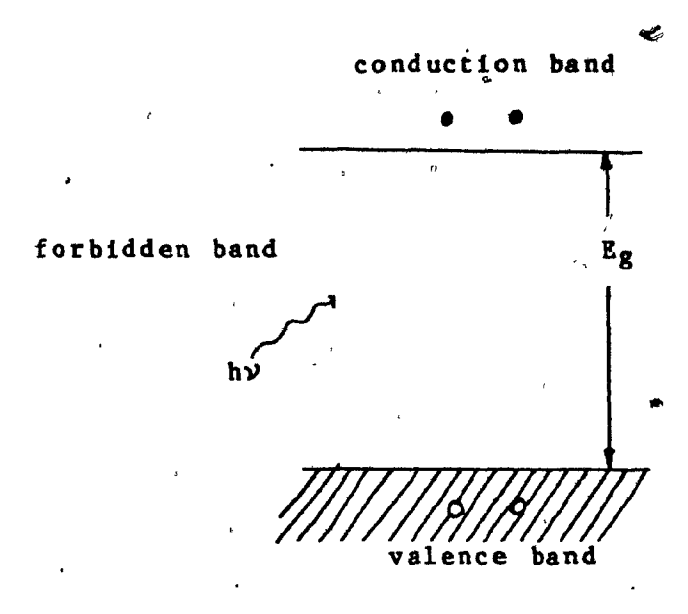


Fig. 2.1

In the simple case of an intrinsic semiconductor material, the conduction and the valence bands are separated by a forbidden band of width $E_{\rm g}$. When this material is irradiated by monochromatic radiation, the width of the

forbidden band determines whether the material is transparent to the radiation or opaque. An incident photon with an energy greater or equal to the gap energy will be absorbed. In terms of the wavelength λ_a of the radiation, the condition for photogeneration of carriers is given by, $\lambda_a \leq hc/E_g$, where h is the Planck's constant, c is the velocity of light and E_g is the gap energy.

2.2 Simplified Treatment of Photoconductivity

Suppose light incident on a plate of semiconductor of length 1, width w and thickness d (Fig. 2.2) generates electron-hole pairs in it at a rate of g per second per unit volume.

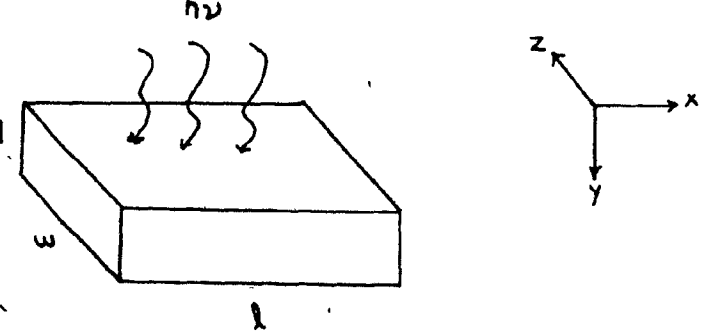


Fig. 2.2

Suppose the length of the sample is sufficiently large and the bias V_0 , applied across the sample, is sufficiently small, that the time required for the carriers to traverse the length, (the transit time) is much longer than the lifetimes τ_n and τ_p of the excess electrons and holes respectively.

Assume further that the recombination rate at the end contacts is the same as that in the bulk of the material.

Suppose the thickness d is large compared with the reciprocal of the absorption coefficient K, so that all the incident radiation, at a flux of J photons per sec per cm² on the sample, is absorbed. The total number of excess electron—hole pairs senerated in the sample is therefore given by JQlw, where Q is the quantum efficiency, usually assumed to be unity. If g is the generation rate per unit volume, then the average value \(\bar{g} \) in the sample is,

$$\frac{1}{g} = \frac{JQ w}{wd} = \frac{JQ}{d}.$$
 (2.1)

The excess electron and hole concentrations on and operate given by $\Delta n = g \tau_n$ and $\Delta p = g \tau_p$ respectively. Hence the increase in conductivity $\Delta \sigma$ is given by,

 $\Delta\sigma=\Delta n e \mu_n + \Delta p e \mu_p$, where μ_n and μ_p are the electron and hole mobilities respectively. Thus in the case under consideration,

$$\Delta \sigma = e \overline{g} (\mu_n \gamma_n + \mu_p \gamma_p)$$
 (2.2)

In many extrinsic semiconductors the mobility-lifetime product of one type of carriers is much larger than that of the other. Hence, under the assumption that $\mu_p \tau_p \gg \mu_n \tau_n$,

$$\Delta \sigma = e^{\frac{A}{8\mu_p}\tau_p} = \frac{e\mu_p\tau_p^{JQ}}{d}. \qquad (2.3)$$

Thus, the photon induced conductivity change varies inversely as the sample thickness.

The relative photoconductive change is given by,

$$\frac{\Delta \sigma}{\sigma_o} = \frac{e\mu_p \tau_p JQ/d}{e(n_o \mu_n + p_o \mu_p)},$$
(2.4)

where n_0 and p_0 are the equilibrium values of the electron and hole concentrations respectively. If the sample is extrinsically p-type for example, then $p_0 \gg n_0$ and

$$\frac{\Delta\sigma}{\sigma_0} = \frac{JQT_p}{p_0d}.$$
 (2.5)

The transit time t_t , the time taken by the holes to traverse the length of the sample under the electric field E, is given by,

$$t_t = \frac{length}{drift \ velocity} = \frac{1}{\mu_p E} = \frac{1/2}{\mu_p V_o}. \tag{2.6}$$

The photoconductive current change ΔI is given by,

$$\Delta I = \Delta \sigma \frac{V_o}{\lambda} \text{ wd} = \frac{-e\mu_p \tau_p JQ}{d} \frac{V_o}{\lambda} \text{ wd} = eJQ(\frac{\mu_p V_o}{\lambda}) w \tau_p$$

$$= eJQ \frac{\tau_p}{\tau_p} \text{ wh}. \qquad (2.7)$$

Let F = incident photon current = Jwl. Then,

$$\frac{\text{photon induced current}}{\text{incident photon current}} = \frac{\Delta I}{F} = eQ \frac{\tau_p}{t_t}$$
 (2.8)

The quantity τ_p/t_t is referred to as the photoconductive gain.

Case b) Thin sample d << 1/K

If the sample thickness d is much less than 1/K, then the number of photons absorbed per unit area is JKd and the number of electon-hole pairs generated per second in the sample is given by JKdQwÅ. Hence the rate per unit volume is,

$$g = \frac{JKQdw!}{Iwd} = JKQ . (2.9)$$

. •

the of a few arms of the Shipping

lease of the good and the second of the seco

till to the second second

Once again assuming $\mu_n T_n < \langle \mu_p T_p \rangle$, then with $\Delta p = g T_p \rangle$, the increase in conductivity is given by,

$$\Delta \sigma = e \mu_{p} g \mathcal{T}_{p} = e \mu_{p} J K Q \mathcal{T}_{p} \qquad (2.10)$$

Thus for a thin film sample, the photon induced increase in conductivity is independent of sample thickness.

The relative change for an extrinsic p-type sample is

$$\frac{\Delta \sigma}{\sigma_o} = \frac{e\mu_p J K Q \tau_p}{e\mu_p p_o} = \frac{J K Q \tau_p}{p_o}. \qquad (2.11)$$

2.3 More Exact Treatment of Photoconductivity

The simplistic assumptions made in the previous section are not always applicable and hence a more rigorous analysis is made in this section.

The continuity equations for holes and electrons are,

$$\frac{d\Delta p}{dt} = g - \frac{\Delta p}{\tau_p} - \frac{1}{e} \quad \text{div } j^+ \qquad (2.12)$$

$$\frac{d\Delta n}{dt} = g - \frac{\Delta n}{\gamma_n} + \frac{1}{e} div j^-, \qquad (2.13)$$

where $g = JK \exp(-Ky)$ is the generation rate of photoexcited carriers and $j^+ & j^-$ are the diffusion current densities of holes and electrons respectively.

The two current densities are given by

$$j^{+} = e\mu_{p}pE - eD_{p}grad p \qquad (2.14)$$

$$j^- = e\mu_n nE + eD_n grad n,$$
 (2.15)

where \mathbf{D}_{n} and \mathbf{D}_{p} are the diffusivities for electrons and holes respectively.

Substituting equations (2.14) & (2.15) into (2.12) & (2.13) gives us

$$\frac{d\Delta p}{dt} = g - \frac{\Delta p}{\tau_p} - \mu_{pp} \text{ divE} - \mu_{p} \text{E.grad p} + D_{p} \text{div grad p} (2.16)$$

t still the second of the second still the second second second second to the second second the second seco

$$\frac{d\Delta n}{dt} = 8 - \frac{\Delta n}{\tau_n} + \mu_n n \text{ divE} + \mu_n E \cdot \text{grad } n + D_n \text{div grad } n \text{ (2.17)}$$

Assuming a low level of illumination, $\Delta p = \Delta n$ we can re-write equations (2.16) & (2.17) as follows:

$$\frac{d\Delta p}{dt} = g - \frac{\Delta p}{\tau_p} - \mu_p p \text{ dive } - \mu_p E. \text{grad } p + D_p \text{div grad } p \text{ (2.18)}$$

$$\frac{d\Delta p}{dt} = g - \frac{\Delta p}{\tau_n} + \mu_n n \text{ divE} + \mu_n E. \text{grad } p + D_n \text{div grad } p \text{ (2.19)}$$

Assuming $\tau_p = \tau_n = \tau$ and combining the two equations (2.18) & (2.19) gives,

$$\frac{d\Delta p}{dt} = g - \frac{\Delta p}{\gamma} + \mu E. \text{grad } p + D \text{ div grad } p ,$$

where
$$\mu = \frac{(p-n)}{(n/\mu_p + p/\mu_n)}$$
 and $D = \frac{(n+p)}{(n/D_p + p/D_n)}$.

It is assumed that the sample is sufficiently long, that any gradient of p along the x direction may be neglected. Accordingly the term uE.grad p maybe taken as zero, since the applied electric field E and the gradient of p are then normal to each other. This further-simplifies the equation to,

$$\frac{d\Delta p}{dt} = g - \frac{\Delta p}{\tau} + D \text{ div grad} \Delta p \qquad (2.20)$$

In the case of the simple rectangular slab under consideration, with steady state conditions, where $\frac{d\mathbf{A}\mathbf{p}}{dt} = 0$

equation (2.20) can be written as,

$$0 = JKexp(-Ky) - \frac{\Delta^p}{\gamma} + D \frac{d^2\Delta^p}{dy^2}$$

or substituting $L^2 = D\tau$,

$$L^{2} \frac{d^{2}\Delta P}{dy^{2}} - \Delta P = -JKTexp(-Ky) \qquad (2.21)$$

and the contract of the same and the

It is shown in Appendix A that this differential equation has the solution for the total number of excess carriers:

$$\Delta P = \frac{J\tau}{1 - K^2L^2} \left[1 - \exp(-Kd) + KL \frac{(KL-d)\exp(-Kd) - (KL+d)}{1 + d \coth \frac{d}{2L}} \right] (2.22)$$

where d = sL/D = s t/L and s is the surface recombination velocity. The change in conductivity is given by,

$$\Delta \sigma = \frac{e(\mu_p + \mu_n)}{d} \Delta P \qquad (2.23)$$

By inspection of equation (2.22) one can see that as Kd goes to zero the value of AP also reduces to zero. This is understandable since K = 0 means that there is no absorption and hence no photoconductivity. Further, as Kd goes to infinity, AP reaches a constant value of

$$(\Delta P)_{a} = \frac{J \Upsilon}{1 + d \cot h (d/2L)^2}$$
.

It can also be shown that equation (2.22) has a maximum value of ΔP as a function of Kd. Physically the reason for the decrease following the maximum with increase of Kd is that as K gets larger, the layer within which carriers are generated gets smaller; this leads to a decrease in the concentration of excess carriers, and hence in photoconductivity because high recombination occurs at the surface. With the maximum of ΔP denoted by ΔP_{max} , curves of ΔP / ΔP_{max} were plotted as a function of Kd, from equation (2.22), for various values of ΔP and four fixed values of d/L. These are shown in Fig. 2.3 through Fig. 2.6 and will be used in connection with the analysis of results in Chapter VI.

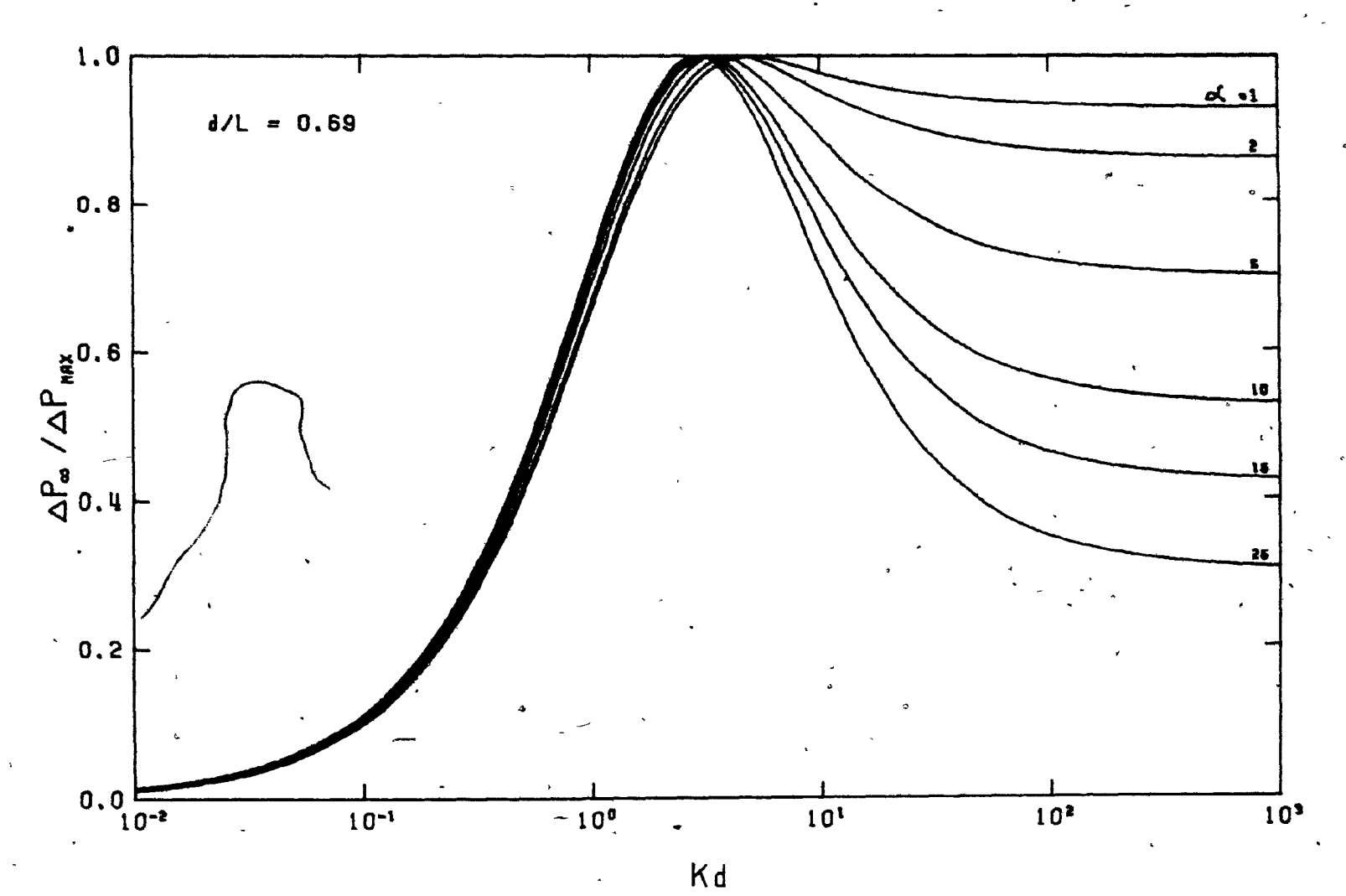
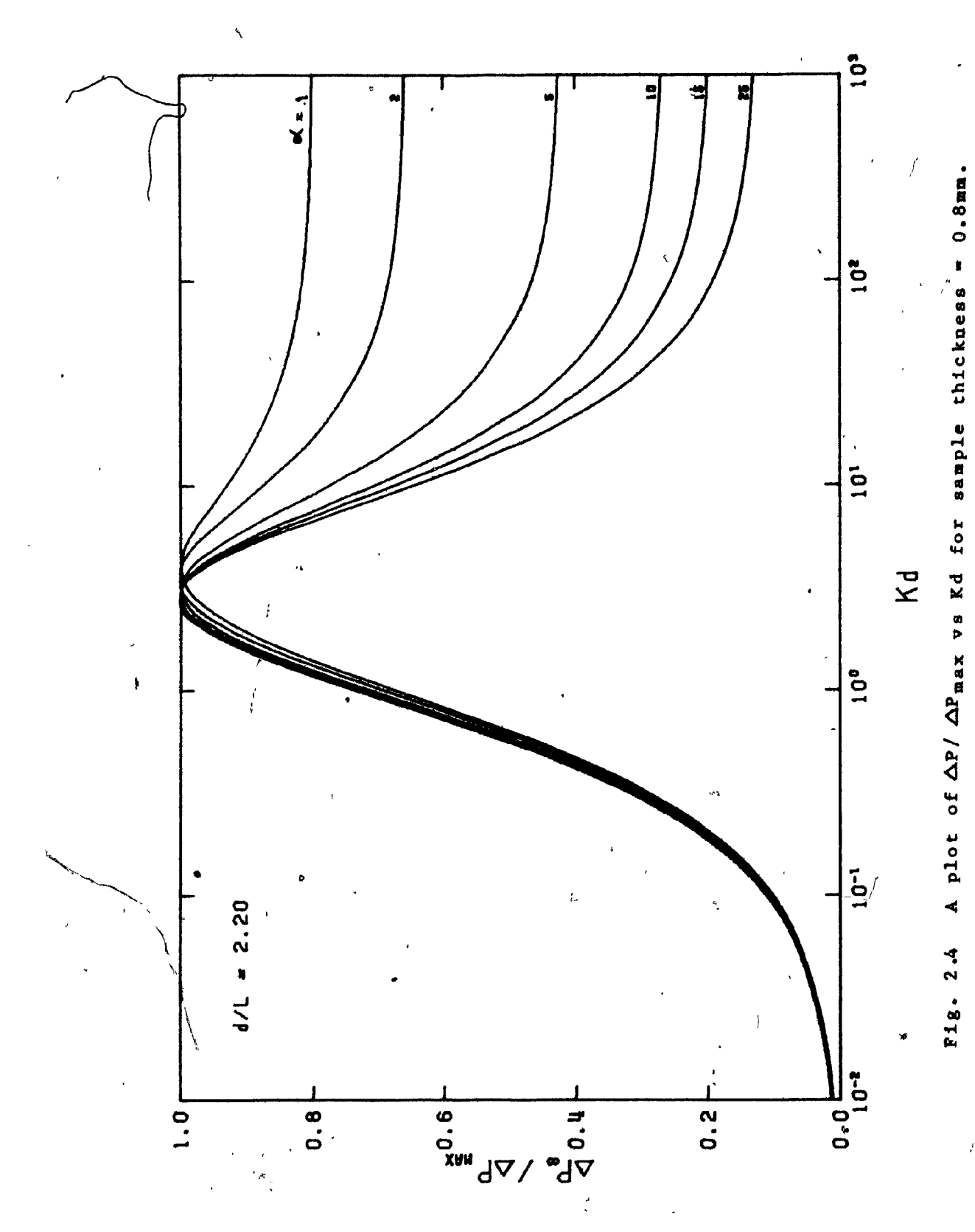


Fig. 2.3 A plot of $\Delta P/\Delta P_{max}$ vs Kd for sample thickness = 0.25mm.



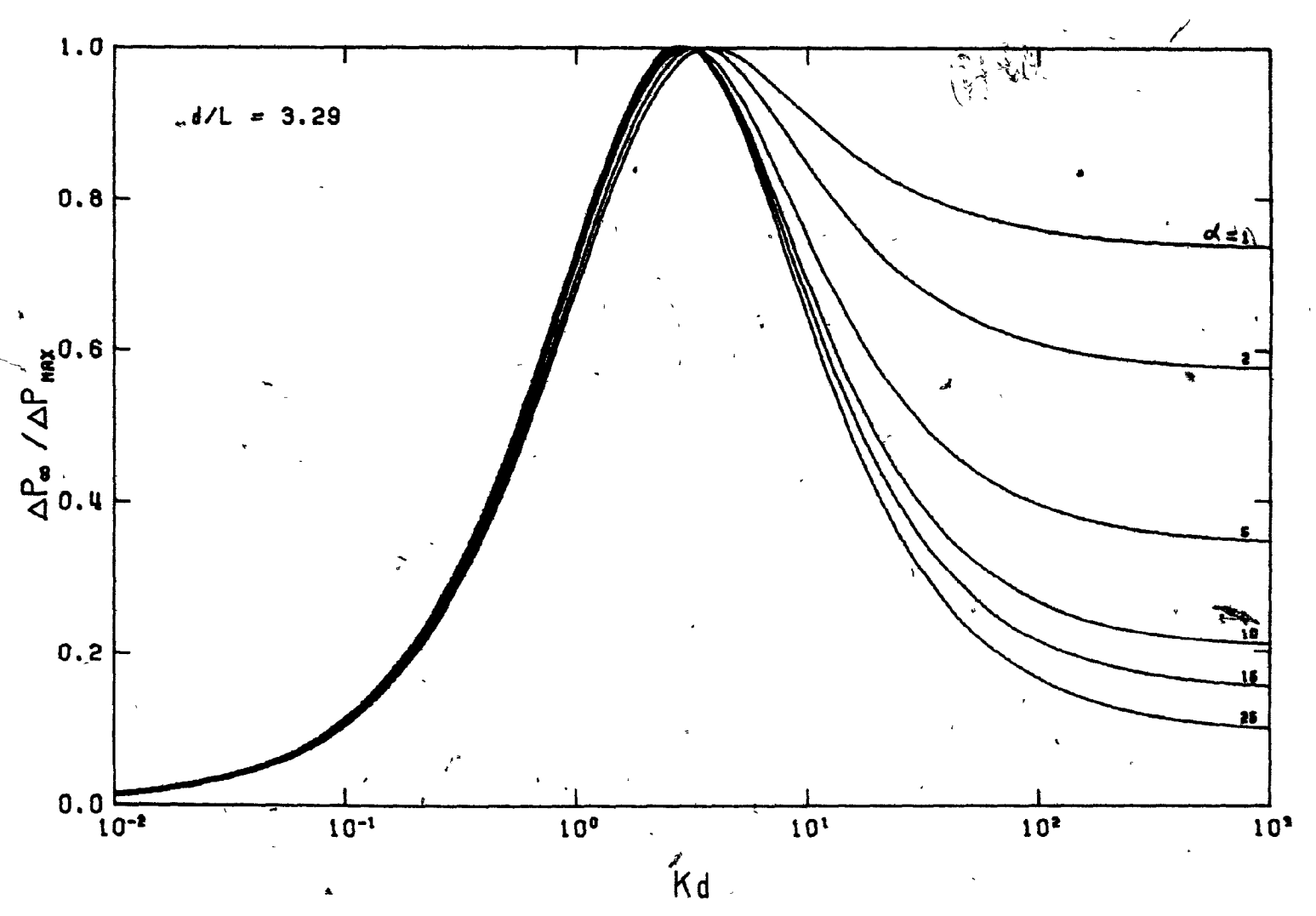
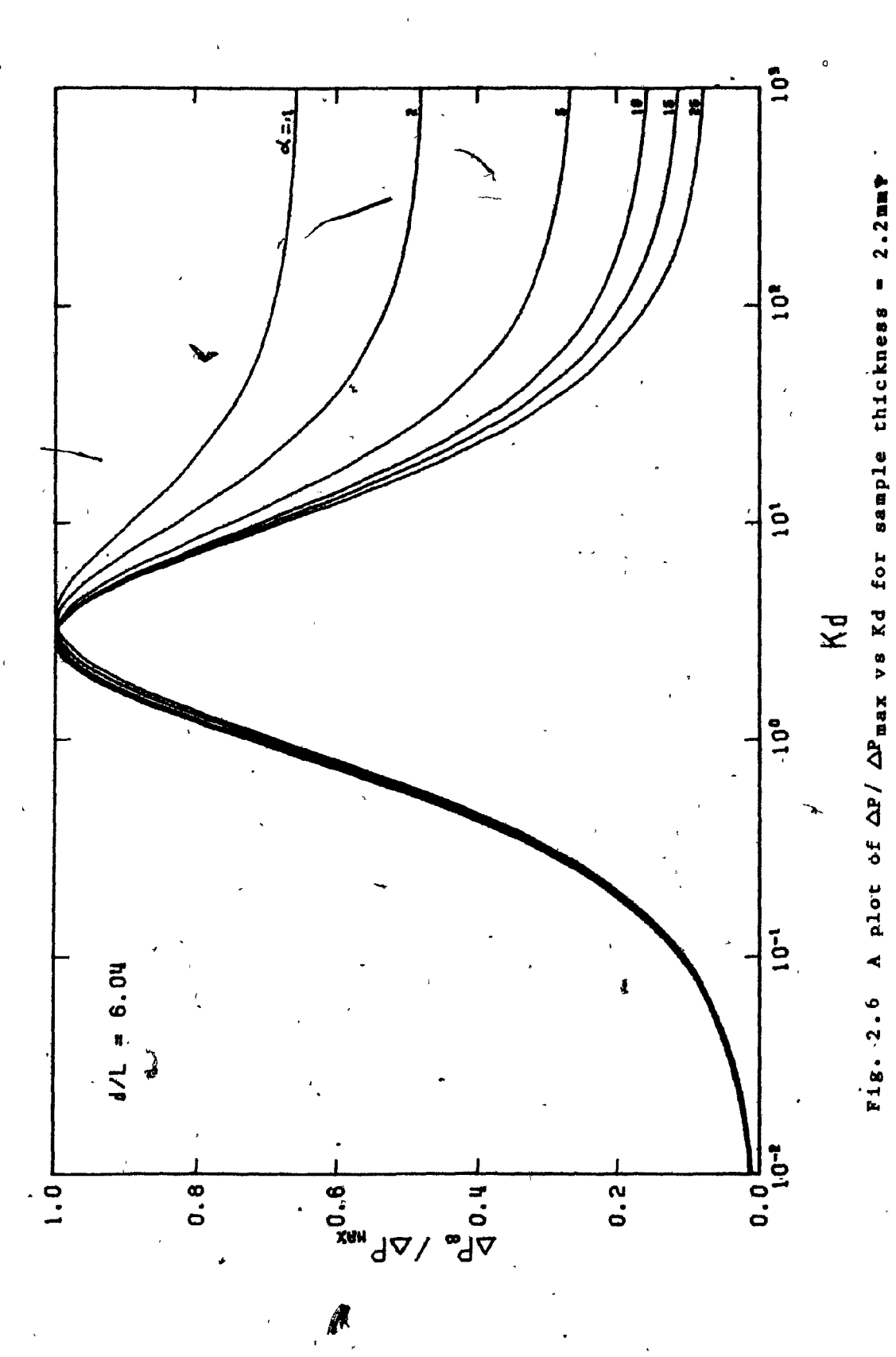


Fig. 2.5 A plot of $\triangle P/\triangle P_{max}$ vs Kd for sample thickness = 1.2mm.



CHAPTER III

TELLURIUM SAMPLE PREPARATION

Measurements of photoconductivity were made on two types of tellurium sample, one in bulk single crystal form and the other in the form of a polycrystalline thin film. In this chapter the techniques involved in preparing both types of sample are described in detail.

3.1 Bulk Samples

The bulk samples were prepared from high quality tellurium monocrystals, grown in our laboratory by the Czochralski method with a starting material of 99.9999% pure tellurium (Cominco single zone refined). The boules consisted of hexagonal prisms pulled parallel to the c-axis and were roughly 2.5 cm in diameter and 10 cm in length.

3.1a Slicing and surface polishing

Thin slices were cut from the ingot using a string solvent saw⁸, with a chromic-hydrochloric acid mixture (composition CrO_3 : $\text{HCl}: \text{H}_2\text{O}$ in the ratio 1 gm: 1 gm: 3 ml). A cutting rate of approximately 1 mm/hr was used, ensuring no pressure on the crystal from the string. This method of cutting avoids structural damage to the material.

Following this, each slice was rinsed first in 30% hydrochloric acid solution and then in distilled de-ionised

water. The slice was next mounted on a polishing block of brass or aluminum with black wax in the following manner. The polishing block and the tellurium slice were heated slowly on a hot plate with the wax applied to the polishing. block. When the wax began to melt the heated tellurium slice was placed on it and allowed to cool. After this, any wax on the surface of the slice was removed using a Q-tip dipped in trichloroethylene (TCE), followed by a rinse in pure ethyl alcohol, which removes any TCE left over. Finally the slice was washed in distilled water.

The slice was then chemically polished in a solvent polishing machine (constructed in our laboratory) using a chromic-nitric acid mixture (composition CrO₃: HNO₃: H₂O in the ratio l gm: 2 gm: 4 ml). The polishing was continued until a smooth and shiny surface was obtained. Next the slice was carefully removed from the polishing block by melting the wax, cleaned in TCE and remounted on the block with the other face exposed. The new face was cleaned with a Q-tip dipped in TCE, rinsed in alcohol and finally in distilled water. This face was now chemically polished until the surface was smooth, shiny and had the approximate required thickness.

3.1b Sample cutting

Rectangular samples about 8 mm x 2 mm in size were cut from the slices using the solvent saw while still mounted on the polishing block. Following the cutting, the samples were washed in TCE, rinsed in alcohol and then in distilled water. After this, they were etched for about a minute in

the chromic-nitric acid mixture, rinsed in 30% hydrochloric acid and finally washed in distilled water and dried.

The samples were cut in the three specific orientations shown in Fig.3.1. Table II gives the dimensions and orientations of all the bulk samples studied. The smallest sample thickness of 0.25 mm was found to be the minimum size which could be fabricated without breakage in the preparation and mounting process.

3.1c Mounting into holder

"The sample holder, as shown in Fig. 3.2 was a rectangular plate of brass 12 mm x 8 mm, having an insulating plate in the middle of which the sample was placed. As shown in Fig. 3.3, one end of the sample was attached to the holder using a low temperature pelting solder (composition Sn: Bi: Sb in the ratio 50: 47:3 gm) which served as an electrical and thermal contact at the same time. The other end of the sample was left free, apart from the #36 gauge copper wire soldered to it acting as the second electrode, enabling expansion and contraction of the sample to take place during temperature changes without introducing internal stresses.

The soldering was the most delicate operation in the sample preparation and great care was needed to avoid any damage to the sample in this process.

3.2 Thin Film Samples

Three thin film tellurium samples were fabricated by evaporating high purity (99.9999+ %) tellurium onto a glass

substrate. Contacts were formed by sputtering gold at the ends as described below.

3.2a Substrate preparation

Pyrex glass slides 18 mm x 18 mm were used as substrates. They were cleaned in detergent solution, rinsed in distilled water and dried in a stream of compressed nitrogen. In each case the slide was placed in a vacuum chamber, shown diagramatically in Fig. 3.4, and pumped down using a rotary vacuum pump, to a vacuum of about 0.1 torr. The glass slide was then subjected to ion bombardment for further decontamination.

3.2b Electrode deposition

After the substrate ion bombardment, the chamber was pumped down to a lower pressure by opening the baffle valve to the diffusion pump. Then argon was introduced into the chamber and the pressure of the gas was maintained at 0.1 torr by manipulating the gas flow and the baffle valve.

Chromium was sputtered on the glass as a first step in obtaining good gold contacts, since a base film of chromium was found necessary to improve the adhesion of the gold film to the glass; a gold film alone will peel off very easily when leads are attached to it. This step was carried out by placing a chromium target under the substrate and applying a high voltage r.f. supply between the target and ground.

[This work was carried out with the assistance of Dr.M.C.Jain]. This results in a film of chromium deposited on the substrate. The pattern of the contact area was defined by a specially shaped mask shown in Fig. 3.5, which

was placed between the substrate and the target and in close contact with the former. With the chromium deposited, the target was then rotated and a gold target positioned for sputtering. The gold film was then deposited on top of the chromium film using the same mask.

3.2c Tellurium deposition

The substrate with the sputtered gold contacts was then placed in the evaporation chamber with the mask shown in Fig. 3.6 placed in close contact with it. The evaporation apparatus is shown in Fig. 3.7. The tellurium was evaporated from a quartz crucible heated by a molybdenum foil heater. The substrate, which was heated by an ordinary soldering iron element attached to the substrate holder, was arranged at a height of about 10 cm above the crucible. Both the heaters were electrically controlled by temperature controllers. Iron-constantan (type-J) thermocouples were used to measure the substrate and crucible temperatures.

The substrate controller was set to 150°C temperature and allowed to stabilize for an hour or two. Then with the shutter closed, the source was heated to a temperature of 430°C, just below the melting point of tellurium. This temperature was chosen in order to keep the evaporation rate sufficiently low. Next the shutter was opened for the required time, depending on the film thickness desired. After the evaporation, the heaters were turned off and the substrate was allowed to cool down naturally in the vacuum system.

Electrical leads were attached to the contact pads using a small pellet of indium pressed onto each gold area. A #36 gauge copper wire was then soldered to the blobs of indium using a low temperature soldering iron. It has been found that indium pressed onto gold in this way makes a good ohmic contact. Other methods of making contact to the gold were found to be unsatisfactory, as the gold film peels off easily upon heating. The sample was then mounted in the sample holder shown in Fig.3.8 secured in the cryostat.

3.2d Au-Te-Au structure

A gold-tellurium-gold sandwich structure, as shown in Fig. 3.9 was also fabricated by alternate deposition of gold, tellurium and gold on a glass substrate. This was done to check if gold forms an ohmic contact with tellurium. This experiment was performed since previous samples made with evaporated aluminum contacts showed extremely high resistance due to the blocking nature of the junction.

,

Bulk Samples used in Photoconductivity Measurements

TABLE II

Sample no.	Dime	ensions	(mm)	Orientation							
Sample no.	Length	Width	Thick.	Bias curr. to c-axis	Plane of illum.						
CZ-77-1/A	9	1.8		parallel	(1010)						
cz-77-1/B	8	2.0	0.25	perpend.	(1010)						
CZ-77-1/C	8	1.9		perpend.	(0001)						
CZ-76-10/A	8	2.1		paralle1	(1010)						
CZ-76-10/B	7	2.5	0.80	perpend.	(1010)						
cz-76-10/c	8	2.0		perpend.	(0001)						
CZ-76-20/A2	9	1.8		parallel	(1010)						
CZ-76-20/B2	8.5	1.9	1.20	perpend.	(1010)						
cz-76-20/c2	9	1.7		perpend.	(0001)						
CZ-76-20/A1	9	2.0		parallel	(1010)						
CZ-76-20/B1	10	1.8	2.20.	perpend.	(1010)						
CZ-76-20/C1	10	1.7		perpend.	(0001)						

The letters A, B, C refer to the sample cuts in the orientations shown in Fig. 3.1.

المرزية

 $(\)$

وجريبية المداجاتين وإواستاك الماك المراد المرابية المؤادين يتحاربون

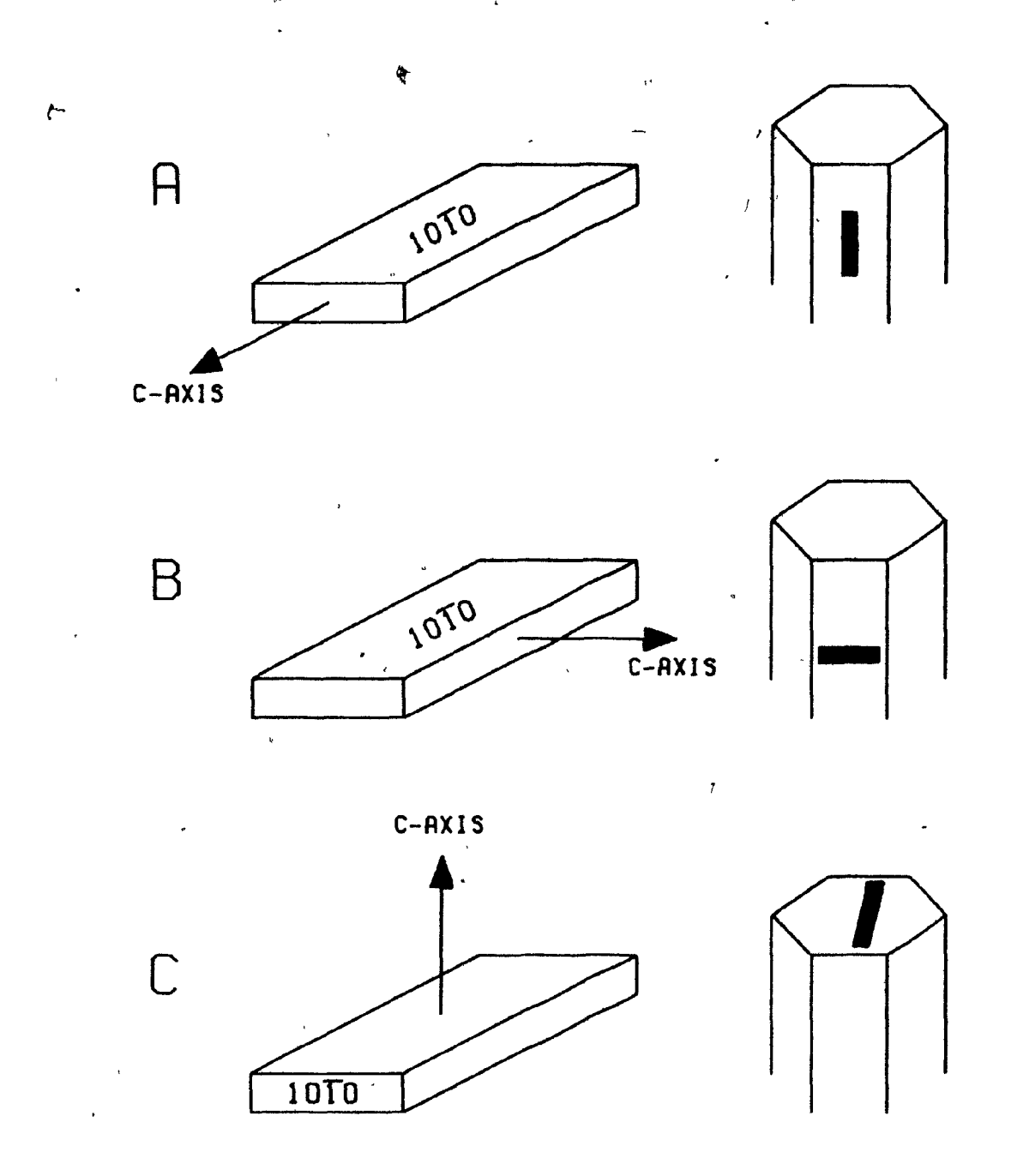


Fig. 3.1 Sample orientations.

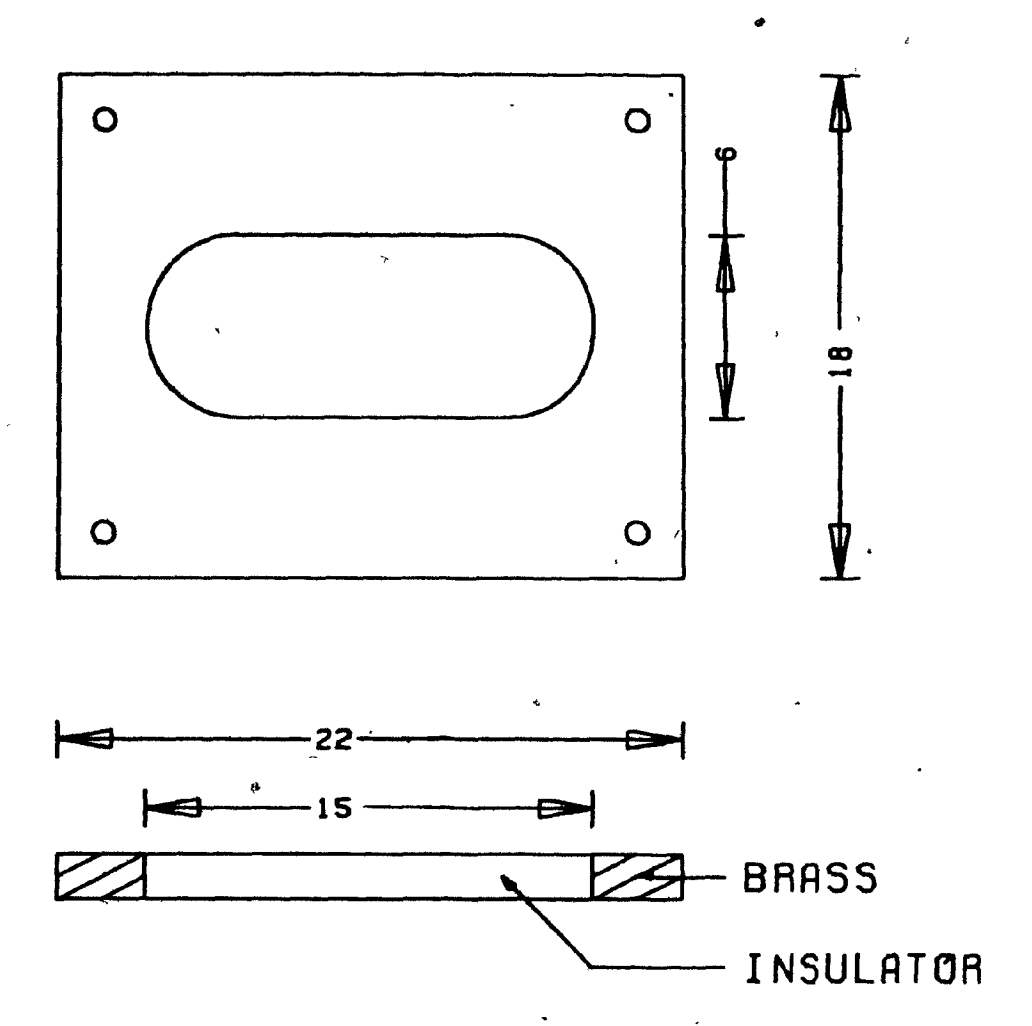


Fig. 3.2 Sample holder (dimensions in mm).

 \bigcirc

P

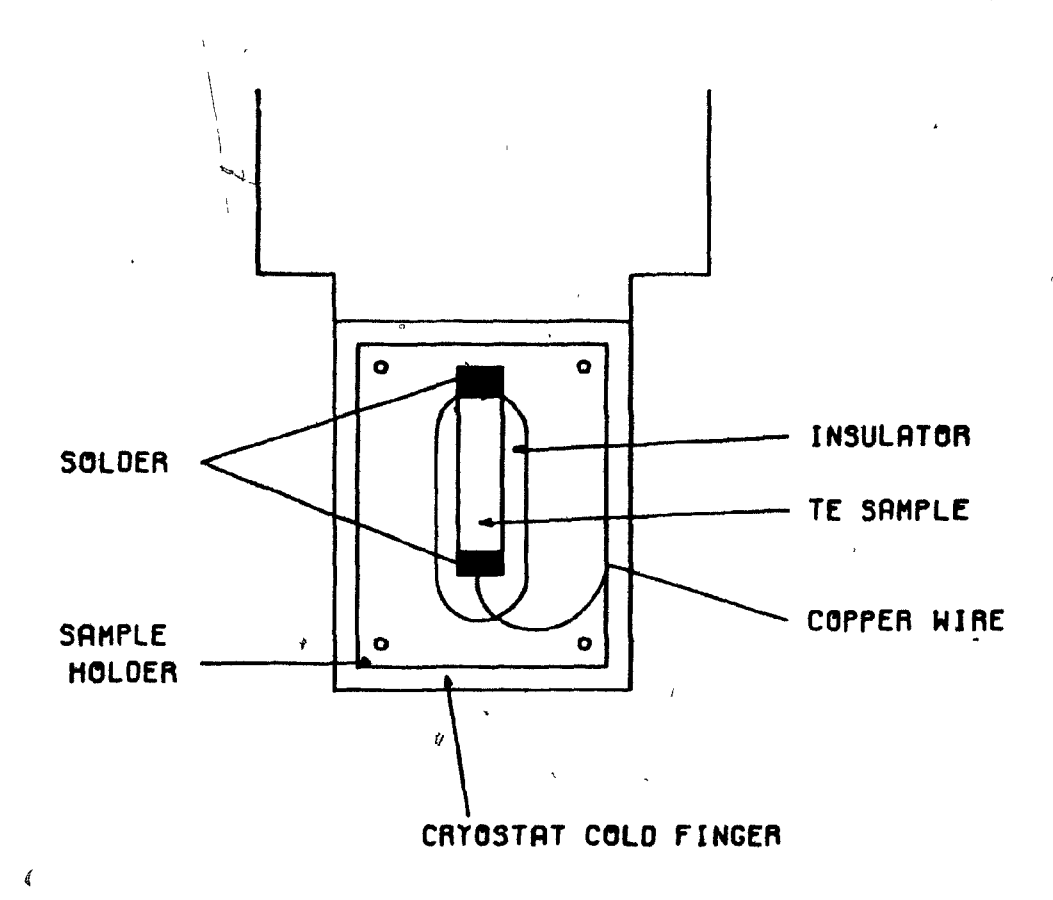


Fig. 3.3 A view of the sample mounted on the sample holder and fixed to the cryostat.

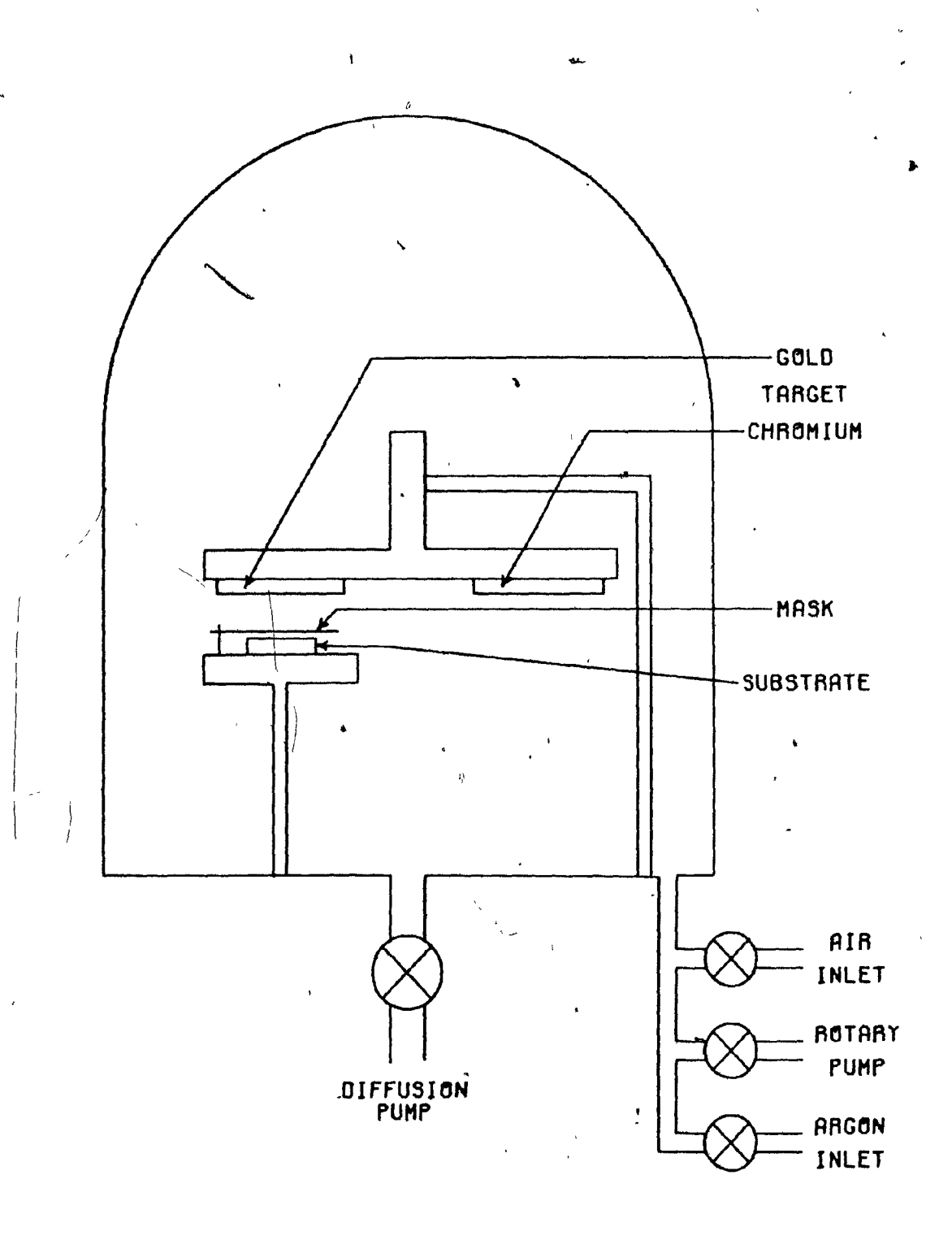


Fig. 3.4 Vacuum chamber setup for sputtering metal contacts.

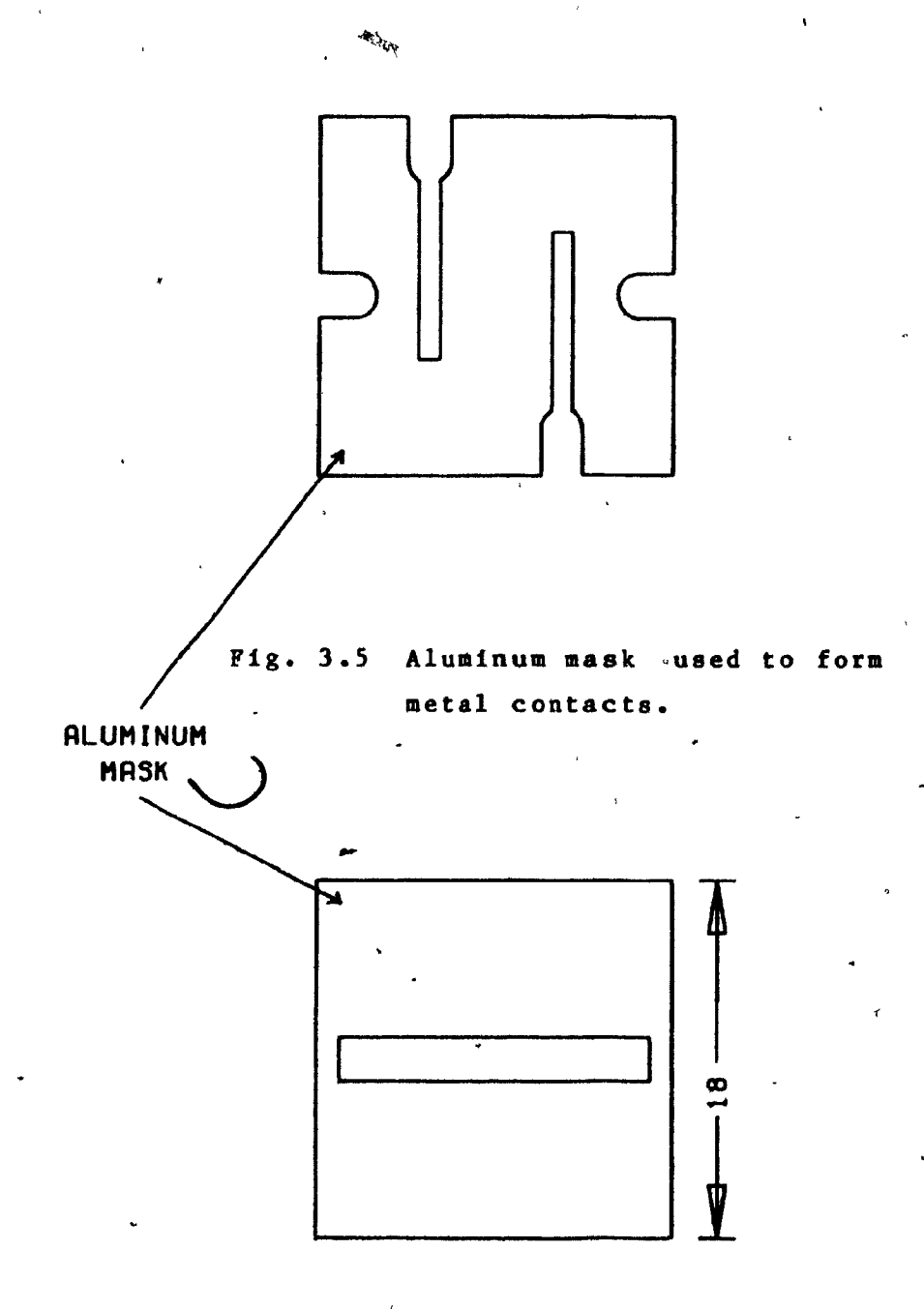


Fig. 3.6 Aluminum mask used to form the tellurium thin film (dimensions in mm).

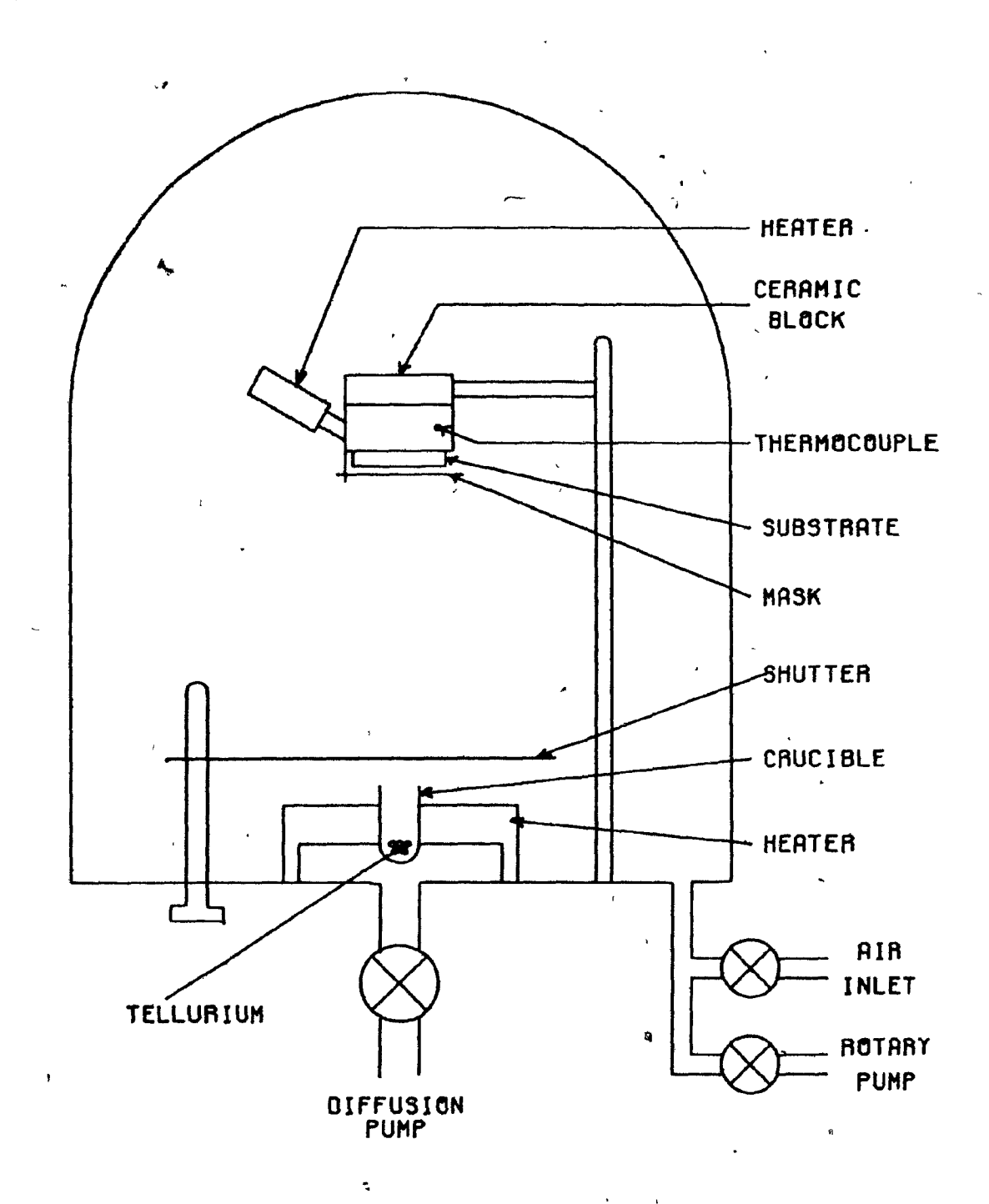


Fig. 3.7 Evaporation of tellurium in the vacuum chamber.

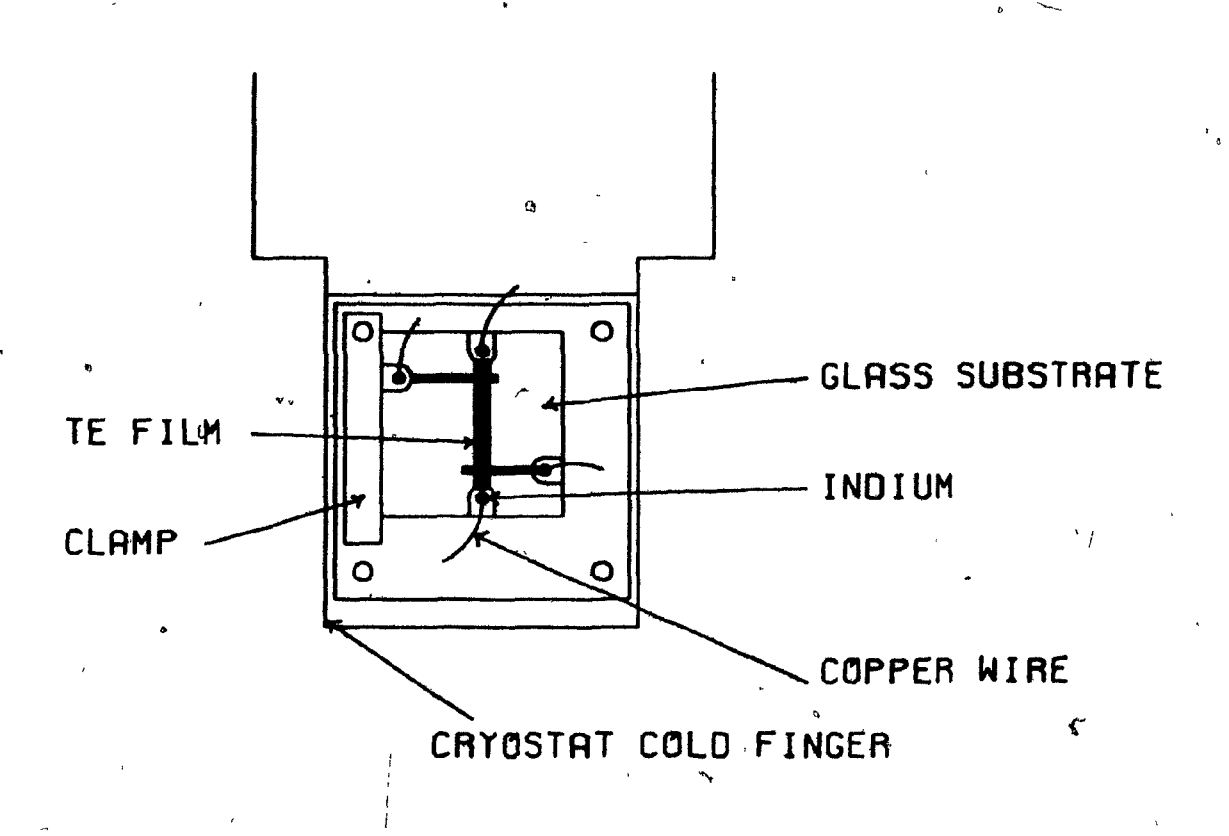


Fig. 3.8 Thin film tellurium sample mounted in the cryostat.

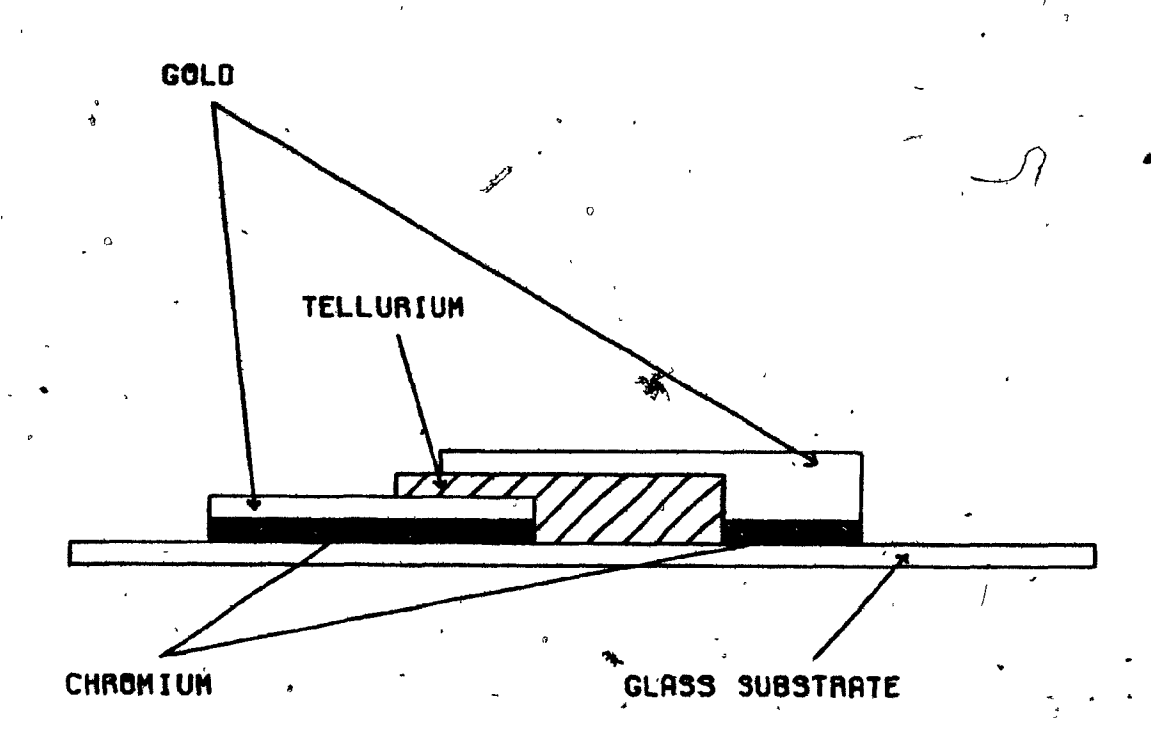


Fig. 3.9 Au-Te-Au structure to check the ohmic nature of the contacts.

CHAPTER IV

MEASUREMENT TECHNIQUES AND APPARATUS.

Photoconductivity measurements were carried out by applying a d.c. bias to the sample, illuminating it with chopped monochromatic radiation and observing the a.c. signal developed across it. In this chapter the measurement procedure and apparatus used are described.

4.1 Monochromatic Illumination Source

A Perkin-Elmer model 13 spectrophotometer was used in the single beam mode to provide monochromatic radiation for illuminating the sample. This unit is shown schematically in Fig. 4.1.

4.la Source unit

The source unit consists of a Nernst glower, through which an electric current is passed to maintain it at a high temperature, yielding almost blackbody radiation. The radiation is collected and focused by a set of mirrors and is interrupted at 13 Hz by a mechanical chopper.

4.1b Monochromator unit

Monochromatic radiation is obtained in the following way. The beam is first passed through an NaCl prism, reflected by a Littrow mirror, passed back through the prism and then focused on a narrow slit inside the unit. This slit allows only a select wavelength band of the dispersed beam to pass through it. Thus the resolution in wavelength can be

improved by reducing the slit width. However this greatly reduces the energy density, so that a compromise has to be reached between resolution and intensity. The monochromatic radiation at this internal exit slit can be switched, by means of a plane mirror in the monochromator optics, either to fall on the thermocouple detector or to come out through an opening in the unit.

4.1c Internal detector and amplifier

A vacuum thermocouple with a KBr window (Reeder Inc.) mounted in the Perkin-Elmer spectrophotometer was used to measure the energy passing through the instrument. The output from this detector is fed into a built-in amplifier, which selectively amplifies the 13 Hz a.c. signal using a reference signal taken from the chopper unit. The chopping of the beam avoids any drift in the amplifier characteristics and any variation of thermocouple output with background radiation.

4.2 External Apparatus

A schematic diagram of the complete experimental setup is shown in Fig. 4.2. The external components of this, consisting of the external optics, cryostat and measuring circuit, are now described.

4.2a Optics

A spherical concave mirror (focal length=10cm) was used to focus the beam diverging from the exit slit of the monochromator onto the sample (Fig.4.3). This mirror was placed near the opening in the back of the monochromator at

an angle of 45° to the beam. The mirror could be tilted and shifted by adjusting screws on its mount.

4.2b Cryostat

A.

An Oxford Instruments cryostat was used to cool the sample to 77 K, at which temperature most of the measurements were made. A cross-sectional view of the cryostat is shown in Fig. 4.5.

The cryostat consists of a long narrow cylinder, through which a flow of coolant is maintained by a rotary vacuum pump. A solid metallic bar at the end of this cylinder serves as the cold finger on which the sample holder is mounted. A hollow brass cylinder fits around the cold finger and acts as a shield. The entire cryostat is surrounded by a metallic jacket. A window (IRTRAN-2) in this jacket allows the beam of light to pass through, as shown in Fig.4.4. The transmission characteristics of the IRTRAN-2 window material are shown in Fig.4.6. The cryostat was evacuated to reduce thermal losses and also to keep the window from fogging.

A thermocouple attached to the cold finger was used to measure the temperature of the sample. Lead-throughs in the cryostat permitted bias supply and output connections to be made to the sample.

4.2c Measuring circuit

The sample was provided with d.c. bias by a battery of 7.5 volts in series with a resistor, whose value was approximately that of the sample. A Princeton Applied Research HR-8 lock-in amplifier was used to measure the output signal from the sample. This is a highly

and the second of the second o

frequency-selective amplifier operating by multiplying the signal and a reference voltage from the chopper and then filtering the product.

4.3 Calibration of the Thermocouple Detector

The vacuum thermocouple detector within the monochromator unit was calibrated to measure the energy density at the sample surface. A calibrated silicon photovoltaic detector was used for this process. The setup is shown schematically in Fig. 4.7.

The silicon cell was placed at the same position where the sample was originally located, in front of the external concave mirror. At each wavelength the plane mirror within the monochromator unit was switched to illuminate first the thermocouple and then the silicon detector. The output of each was noted down. The total energy incident on the silicon cell was found by looking up its calibration chart at that wavelength. The area of illumination of the silicon detector was measured in the visible range and assumed to be the same in the infrared range. The energy density was obtained by dividing the total energy by the area of illumination. Thus a relation between the energy density at the sample surface and the thermocouple output was obtained at each wavelength. The thermocouple was calibrated from *0.65 micron to 1.0 micron by this method for a fixed slit width of 0.25 mm. The resulting curve is shown in Fig. 4.8. The thermocouple detector is a heat sensing device and hence its output is independent of the wavelength of radiation.

()

The calibration over the range 0.65 - 1.0 micron supports this assumption and hence the same curve has been extrapolated up to 5 microns.

4.4 Photoconductivity Measurement

The sample in the evacuated cryostat was placed in front of the concave mirror. The source was switched on and the current through the glower was slowly increased to the preset value. Liquid nitrogen was pumped through the cryostat and the flow was regulated to maintain a slow rate of cooling - around 5 K per min. A rapid cooling causes thermal damage to the sample and produces excessive imperfections in it.

Once the sample was cooled to 77 K, it was illuminated with the monochromatic radiation and the signal developed across it was measured. The distance between the sample and the concave mirror was then adjusted, so that a maximum signal was obtained.

All the measurements' were carried out with plane polarised radiation obtained with a Cambridge Optics Co. wire grid polariser placed between the chopper and the monochromator. Measurements were done at several points in the wavelength range 1 - 5 microns, noting the output of the vacuum thermocouple and the signal from the tellurium sample. An upper limit of wavelength of 4.5 microns was found, beyond which there was a sharp drop in sensitivity. The lower limit of 1 micron was due to the reduction in transmitted energy from the monochromator.

Variation of photoconductive sensitivity with temperature was obtained, by noting the signal output from the sample for the wavelength corresponding to the peak sensitivity at different temperatures. The temperature change was obtained by allowing the cryostat to warm up after the flow of liquid nitrogen had been stopped.

Variation of photoconductive sensitivity with chopping frequency was also obtained at the wavelength of maximum sensitivity. In order to do this an external d.c. motor with a rotating disc was used. This disc was placed between the source unit and the monochromator unit. A reference signal was obtained through a photocell which was also illuminated by the light interrupted by this chopper.

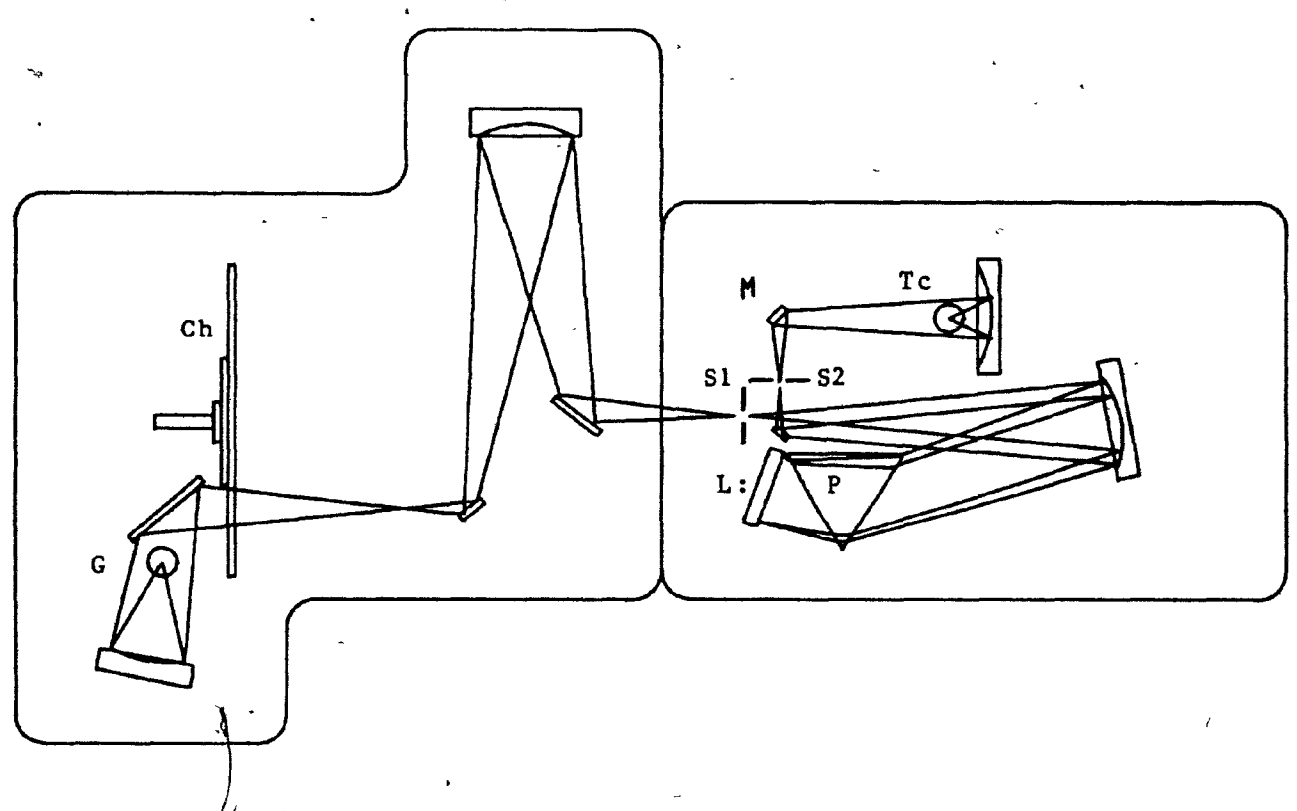


Fig. 4.1 Schematic diagram of the spectrophotometer.

G - Nernst glower, Ch - Chopper, sl,s2 - slits

L - Littrow mirror, P - Prism, M - Mirror

T_C - Thermocouple detector.

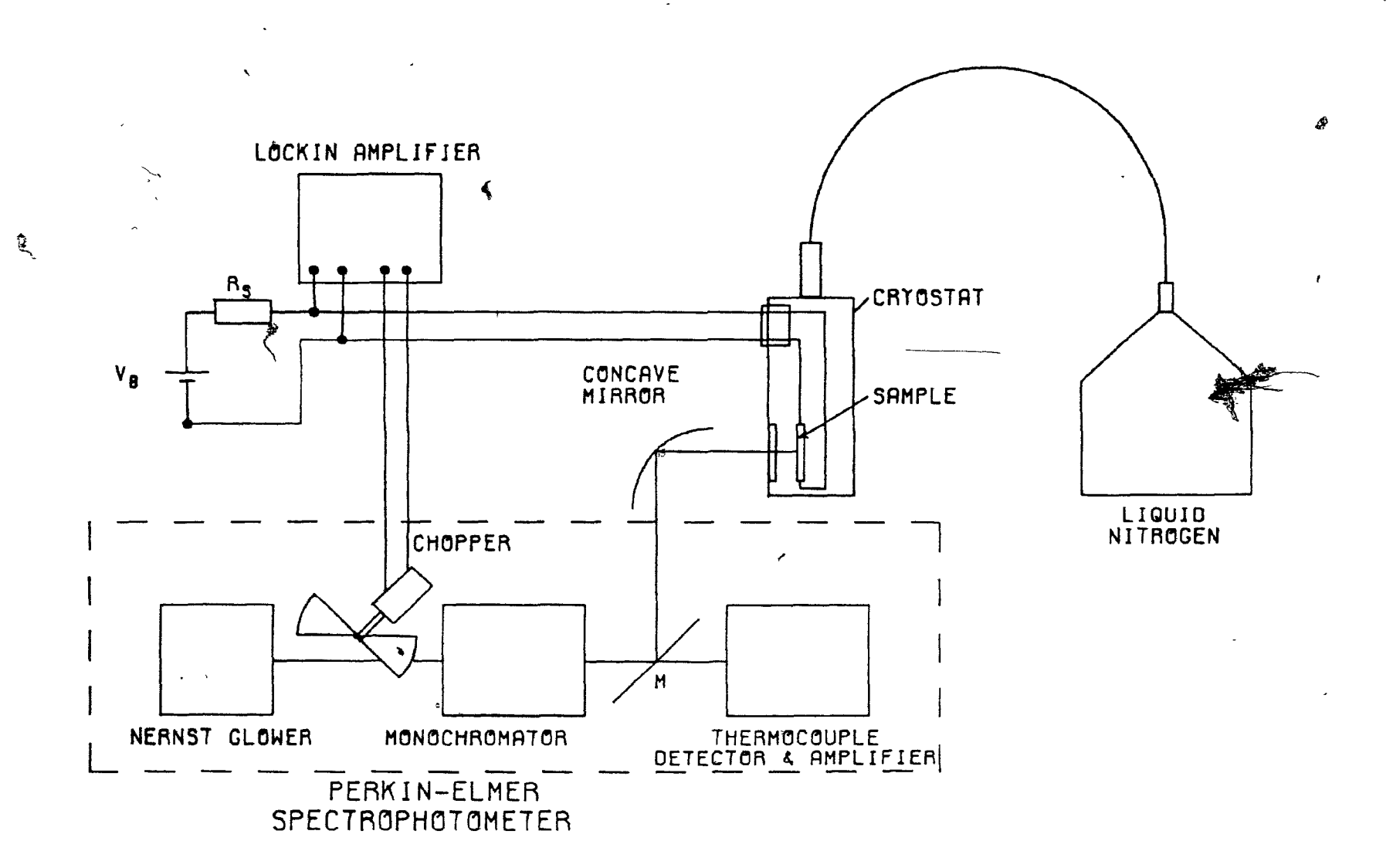


Fig. 4.2 Schematic diagram of the experimental setup to measure photoconductive sensitivity.

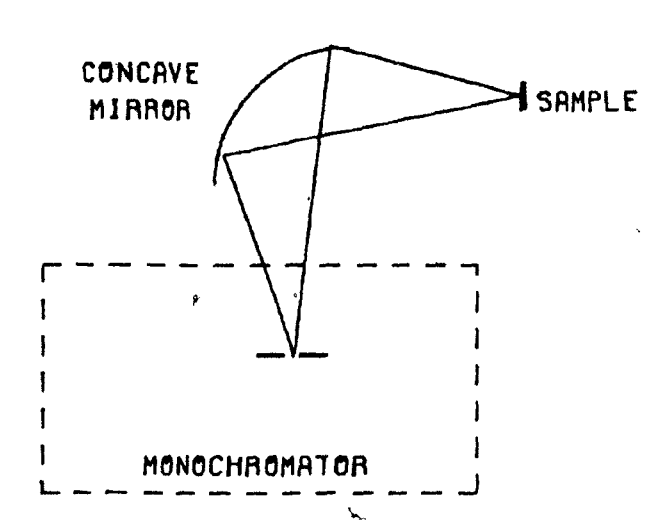


Fig. 4.3 External optics to focus the beam of radiation onto the sample.

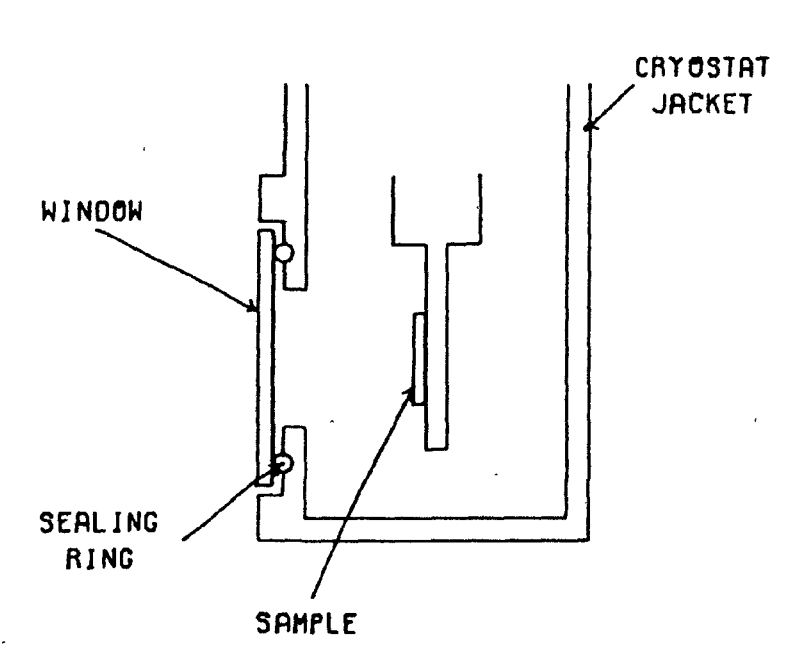
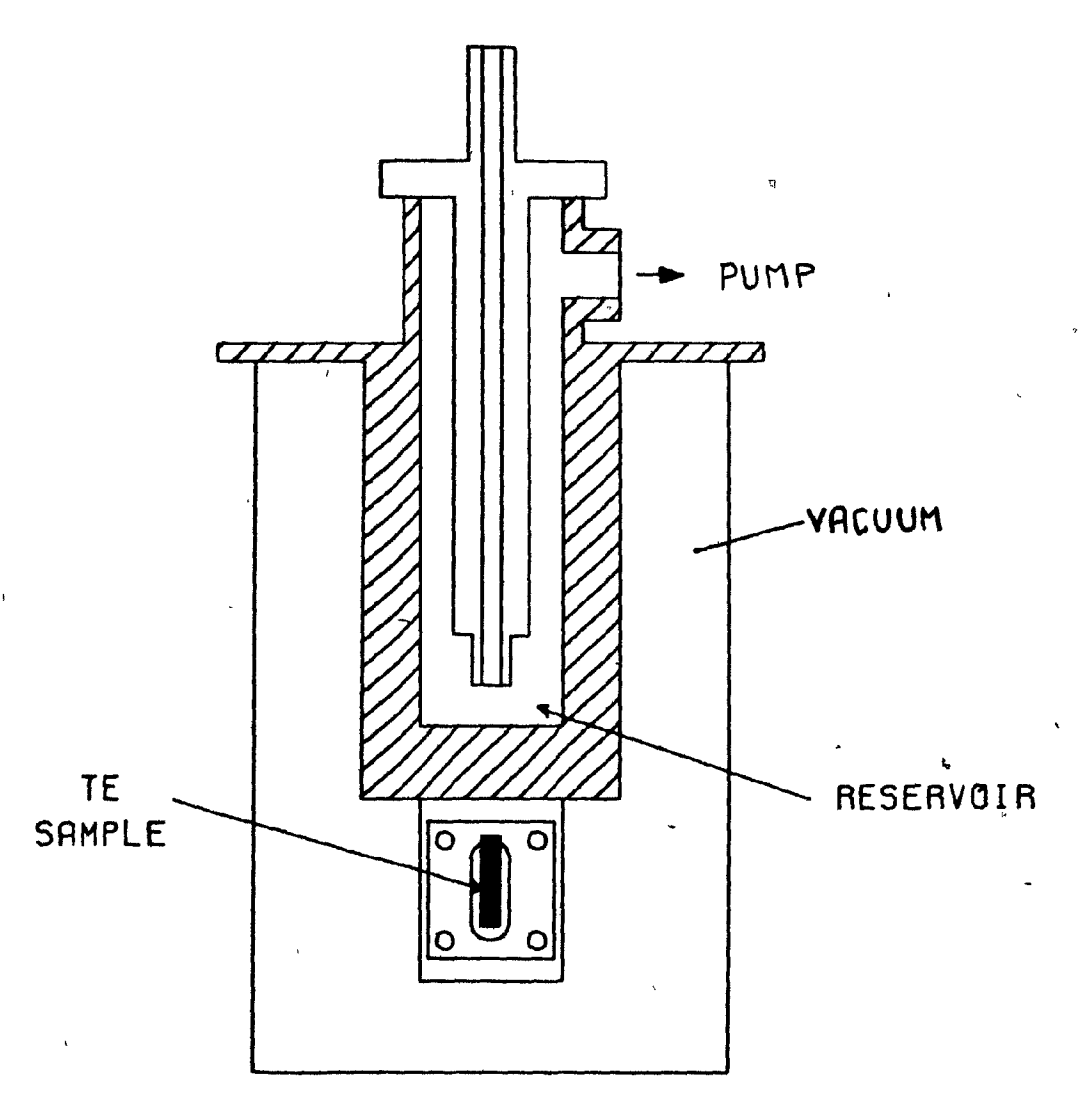


Fig. 4.4 Cross-sectional view of the cryostat showing the window mounting.

nijida kan ana propinsi dingelejadiya





Front view of the cryostat.

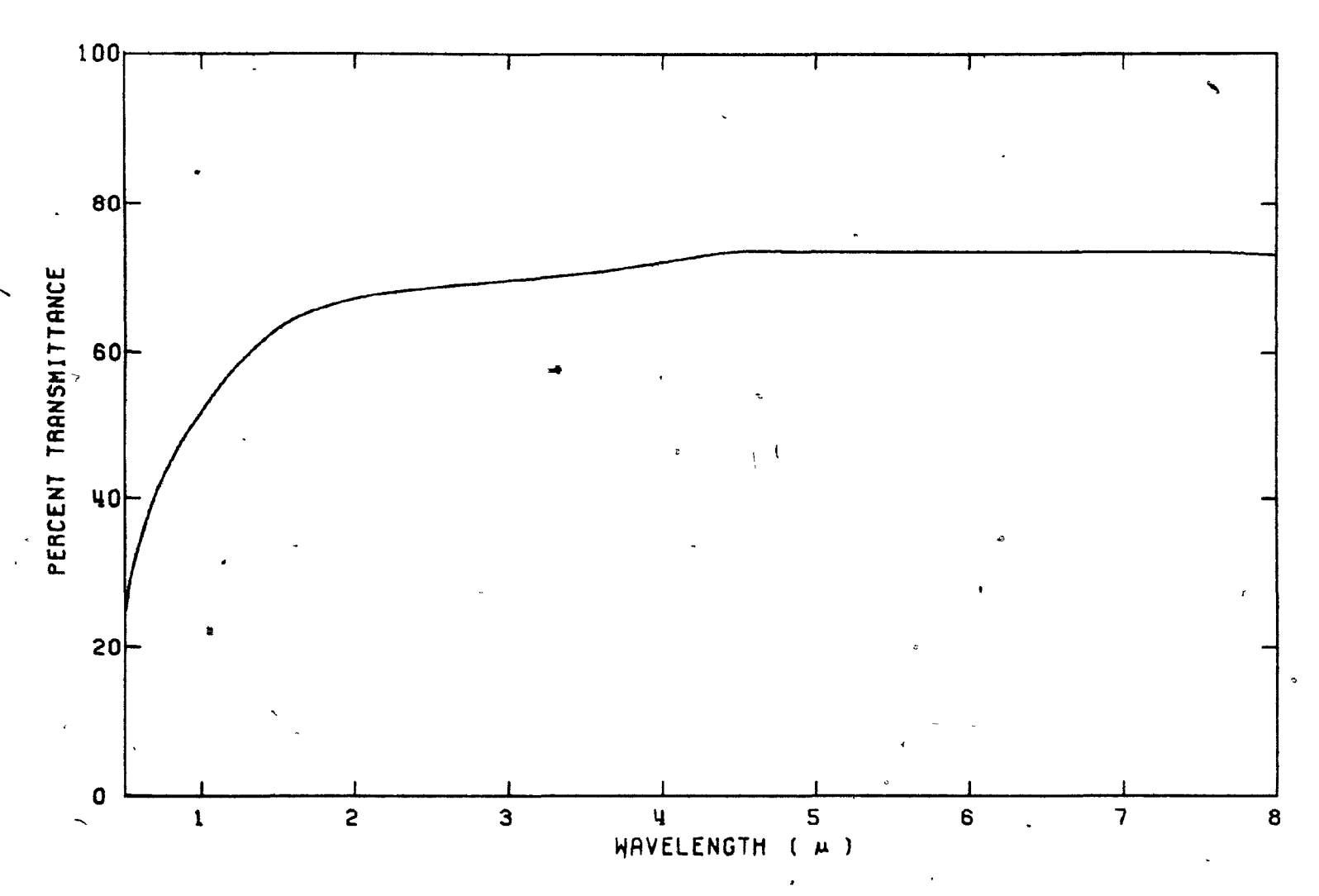


Fig. 4.6 Transmission characteristics of IRTRAN-2 window. (taken from KODAK data sheets)

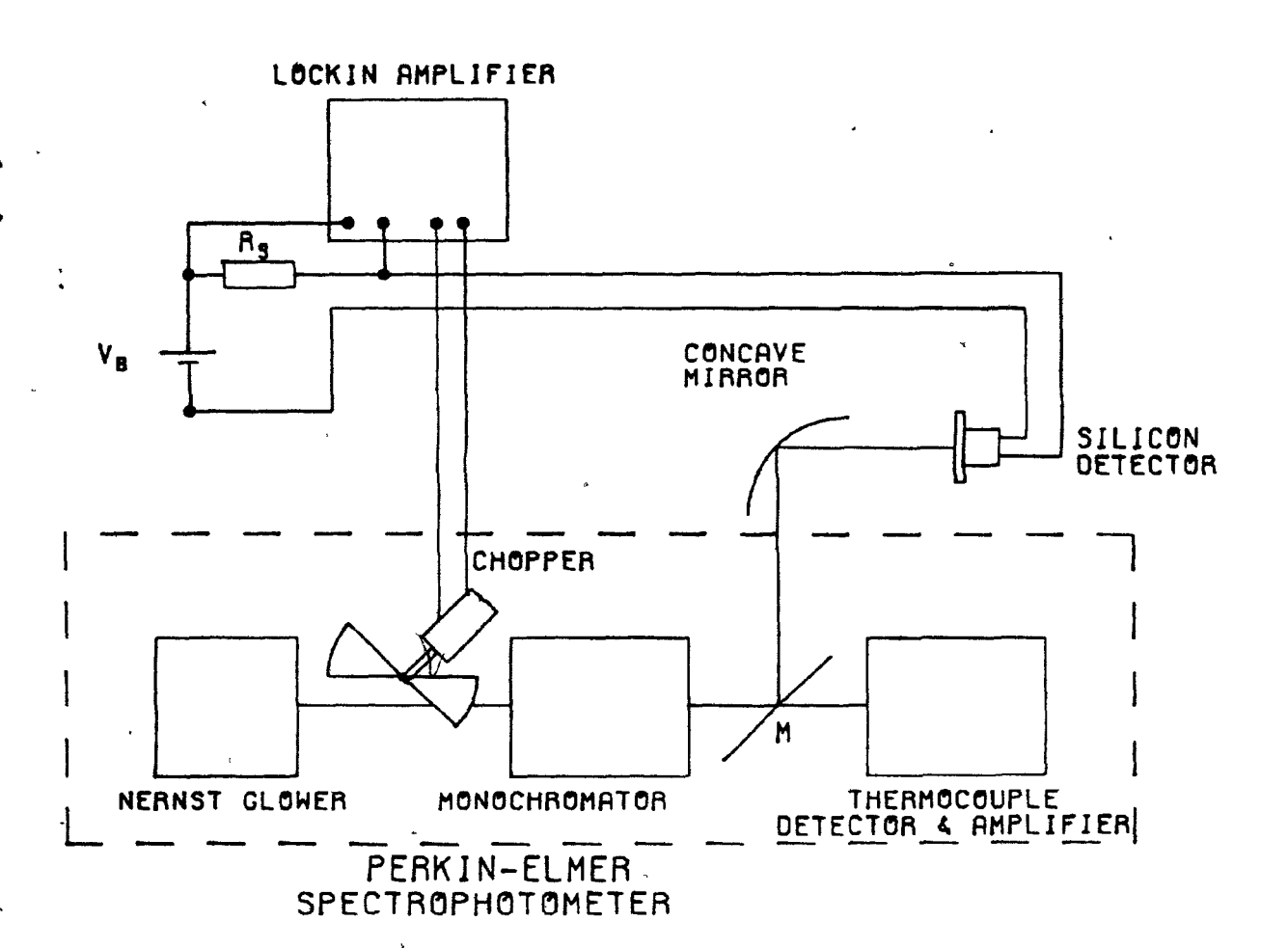


Fig. 4.7 Experimental setup to calibrate the thermocouple detector of the spectrophotometer.

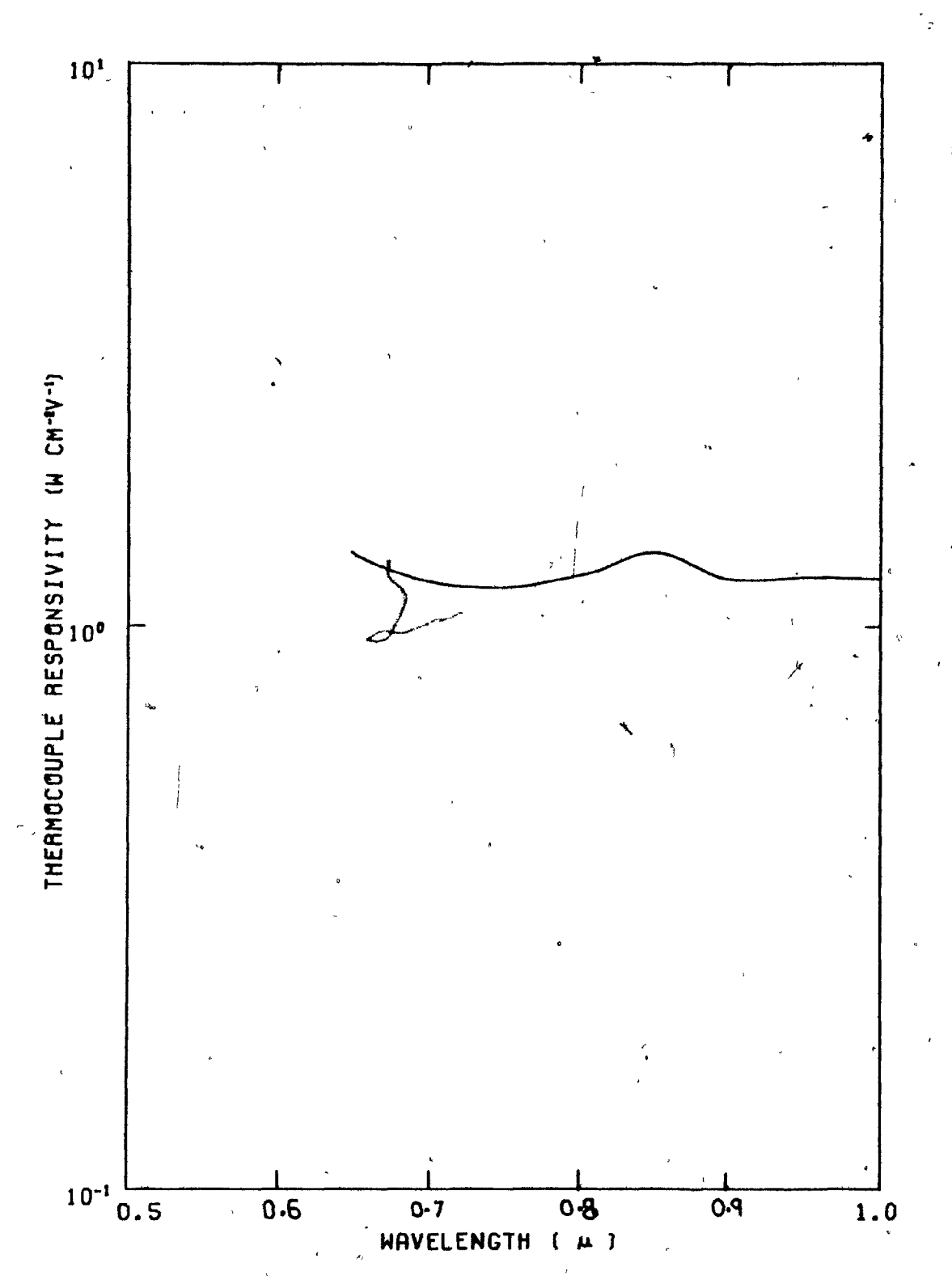


Fig. 4.8 Calibration curve of the thermocouple detector.

CHAPTER V

PHOTOCONDUCTIVITY RESULTS

In this chapter the results of the photoconductivity measurements carried out as described in Chapter IV, are presented for the two types of sample.

A schematic diagram of the measuring circuit is shown in Fig. 5.1. The battery of V_b volts applies a d.c. bias of V_0 to the sample of resistance R_p in series with a resistor of value R_s . The change in the voltage across the sample due to the incident infrared energy is ΔV . It is apparent from this diagram that the relative change in conductivity is given by $\frac{\Delta C}{C_0} = \frac{\Delta V}{V_0} \frac{R_s + R_p}{R_s}$.

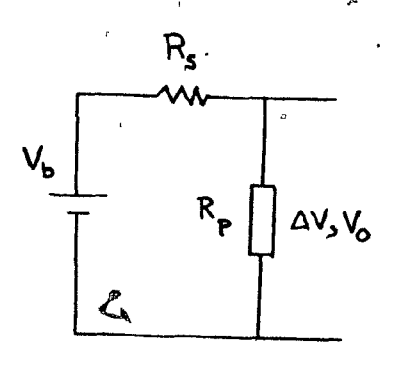


Fig. 5.1

The photoconductive sensitivity is hereby defined as the relative change in conductivity per unit incident energy flux Je, that is $\frac{\Delta G}{G_O J_e}$ or $\frac{\Delta V}{V_O J_e} \frac{R_S + R_p}{R_S}$.

This quantity is plotted for the various samples with $J_{\mathbf{e}}$ calculated from the thermocouple output and its calibration curve.

5.1 Bulk Samples

In the case of bulk tellurium samples the variation of photoconductive sensitivity with a) wavelength,

b) temperature and c) modulation frequency was measured. The monochromator slit width was held constant at 0.25 mm throughout the measurements.

5.la Variation with wavelength

Log-linear plots of photoconductive sensitivity at 77 K versus the wavelength of irradiation for the samples cut in the 'A' orientation (see Fig. 3.1 for the various orientations) is shown in Fig. 5.2 & Fig. 5.3 respectively for the E vector parallel and perpendicular to the c-axis. Similar plots for the samples cut in the 'B' orientation are shown in Fig. 5.4 & Fig. 5.5 and for the 'C' orientation (E perpendicular to c-axis only) in Fig. 5.6.

It is noted that as the wavelength is reduced, the sensitivity increases to a maximum value followed by a decrease. This decrease is gradual for E parallel to c-axis, but is initially steep and then gradual for E perpendicular to c-axis. This difference of shape is brought out more clearly in Fig. 5.7 where the results for the two polarisations of E are compared directly.

It is also noted that on the short wavelength side of the maximum there is a marked dependence on thickness, with an increase in sensitivity with a decrease in thickness. In this region undufations superimposed on the gradual decrease are also noted for some of the samples.

With orientations 'A' & 'B' the monochromatic radiation was incident on the (1010) plane, while with orientation 'C' the (0001) plane was illuminated. Figs. 5.8 & 5.9 show the photoconductive sensitivity for the three sample

orientations A, B and C with sample thicknesses of 0.25 mm and 0.8 mm respectively. Comparison of these two figures indicates that there is not a clear difference in photoconductivity between the three orientations.

5.1b Variation with temperature

Due to the low level of the photoconductive signal, it was only possible in the present work to measure the variation of photoconductivity with temperature at the wavelength of maximum sensitivity. The results for the sample CZ-76-10/B are shown in Fig. 5.10. It is noted that there is a sharp drop of sensitivity above 120 K. Since sample resistivity was found to be approximately constant in the range from 77 to 120 K, this decrease in photoconductivity must be due to a decrease of lifetime with increasing temperature.

5.1c Variation with frequency of modulation

The variation of photoconductivity with the frequency of chopping of the infrared beam, measured in the manner described in Chapter IV, is shown in Fig. 5.11 for the sample CZ-76-10/B at the wavelength of maximum sensitivity and 77 K. The slope of the decrease was found to be approximately 20dB/octave which suggests a simple exponential decay of carriers with time. The time-constant of this decay is approximately 1.6 msec.

5.1d Estimate of detectivity

()

Some preliminary noise measurements were made on a sample 0.1 mm thick at RCA Research Laboratories, St. Anne de Bellevue, Que., with the kind assistance of

Dr. E.J. Fjarlie. The noise voltage was measured across the unilluminated sample at 77 K, with the same bias as used in the photoconductivity measurements. This noise was measured at a frequency of 23 Hz and a bandwidth of 5.7 Hz. The noise equivalent power (NEP) calculated from this was 1.86×10^{-9} watt at a wavelength of 1.94 microns. The corresponding detectivity D* was 4.46×10^7 cmHz $^{\frac{1}{2}}$ watt $^{-1}$. This value extrapolated to 3.7 microns, the wavelength of maximum sensitivity, gives a detectivity of 2×10^8 cmHz $^{\frac{1}{2}}$ watt $^{-1}$ at 23 Hz.

5.2 Thin Film Samples

Three thin film tellurium samples were fabricated, as described in Chapter III, with thicknesses of 0.8, 3.65 and 6.5 microns. The variation of photoconductivity with wavelength is shown in Fig. 5.12. It is noted that the maxima occur at much shorter wavelengths compared to those for bulk samples. The other notable difference is the increase in sensitivity with increase in thickness as opposed to the decrease observed for the bulk samples.

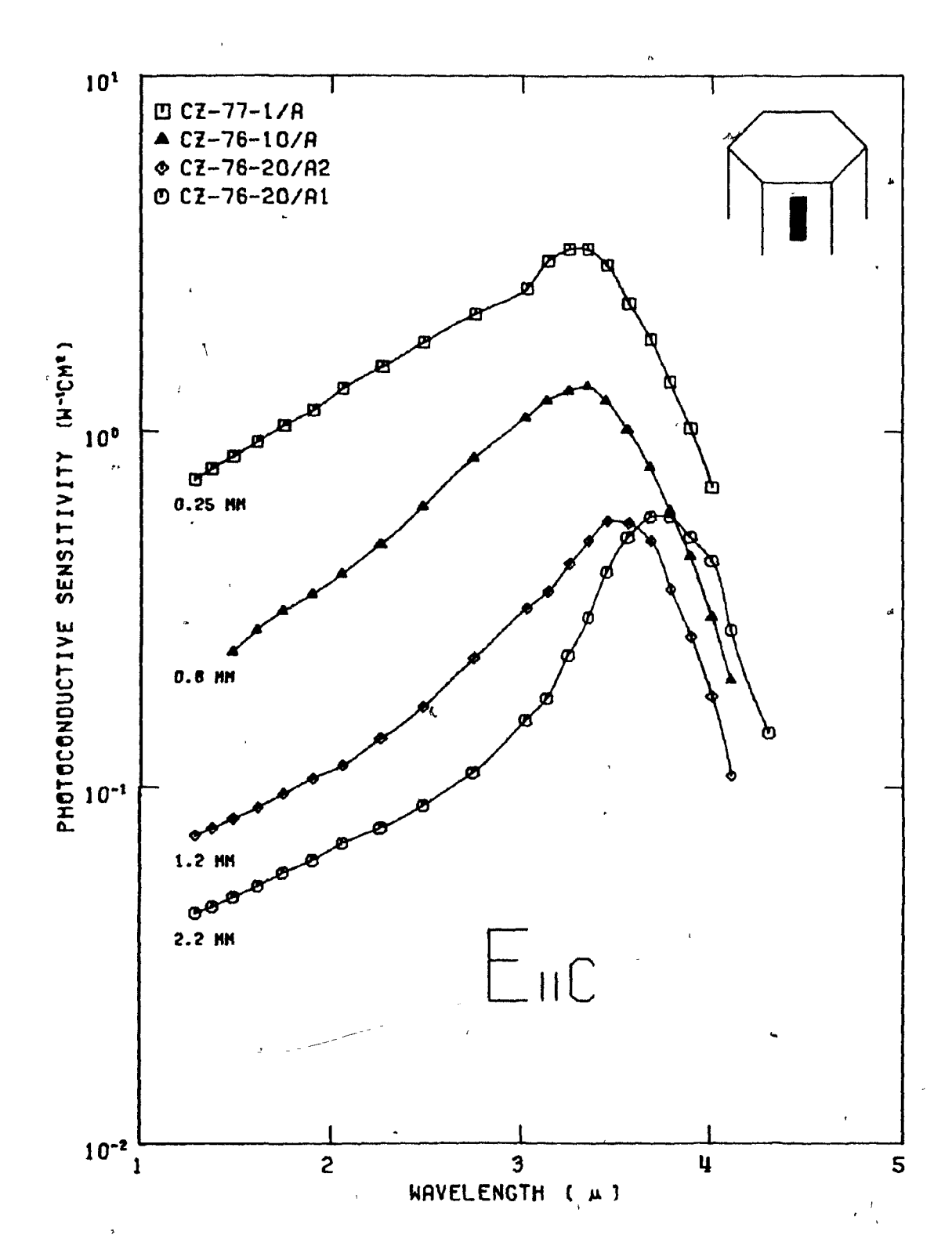


Fig. 5.2 Photoconductive sensitivity vs wavelength for sample orientation 'A' with Elic.

()

+)

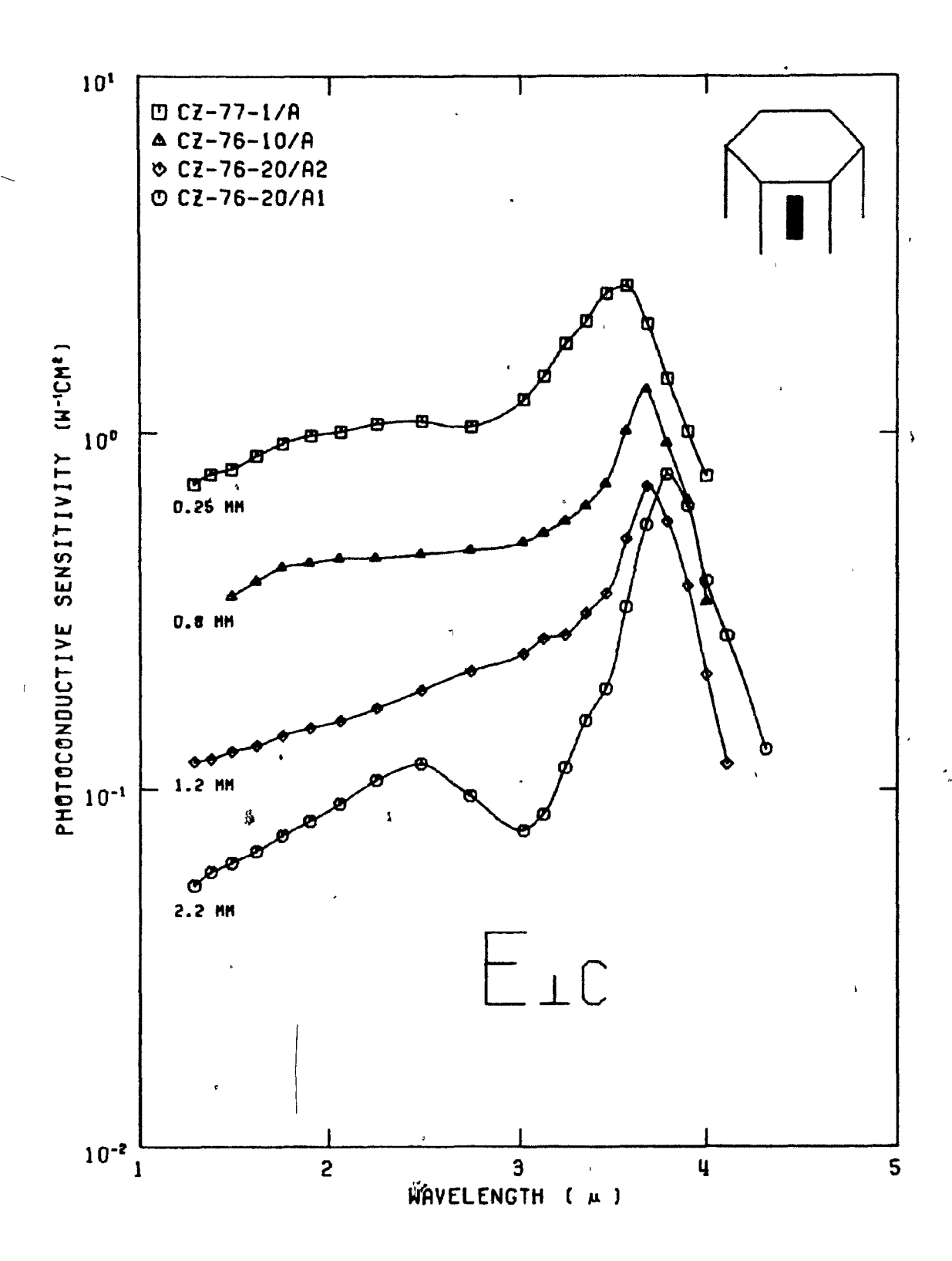
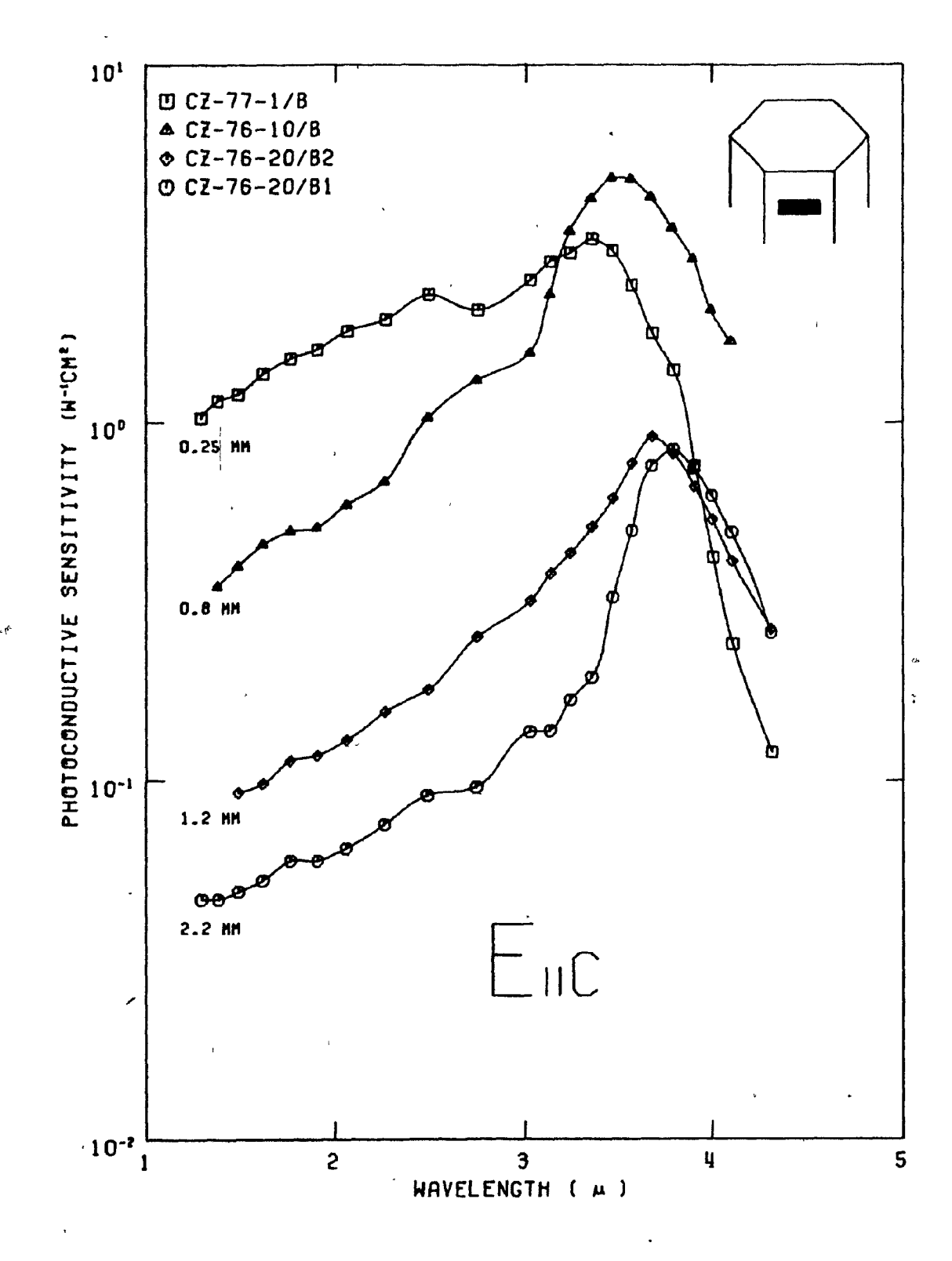


Fig. 5.3 Photoconductive sensitivity vs wavelength for sample orientation 'A' with Eic.



Photoconductive sensitivity vs wavelength for sample orientation 'B' with Ellc.

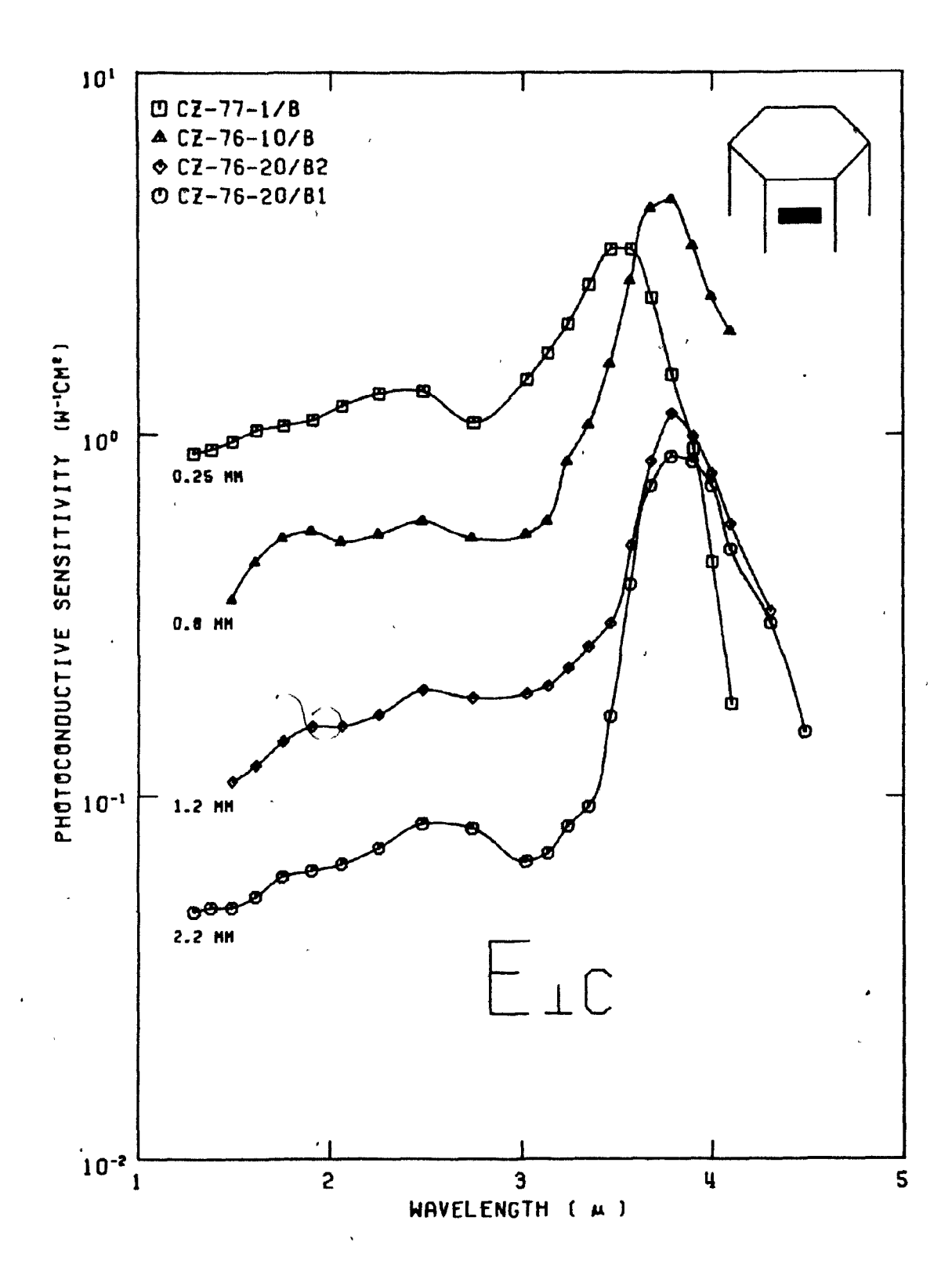


Fig. 5.5 Photoconductive sensitivity vs wavelength for sample orientation 'B' with Eic.

»,

...

granisa da maria da m

- "Followedder Salukure

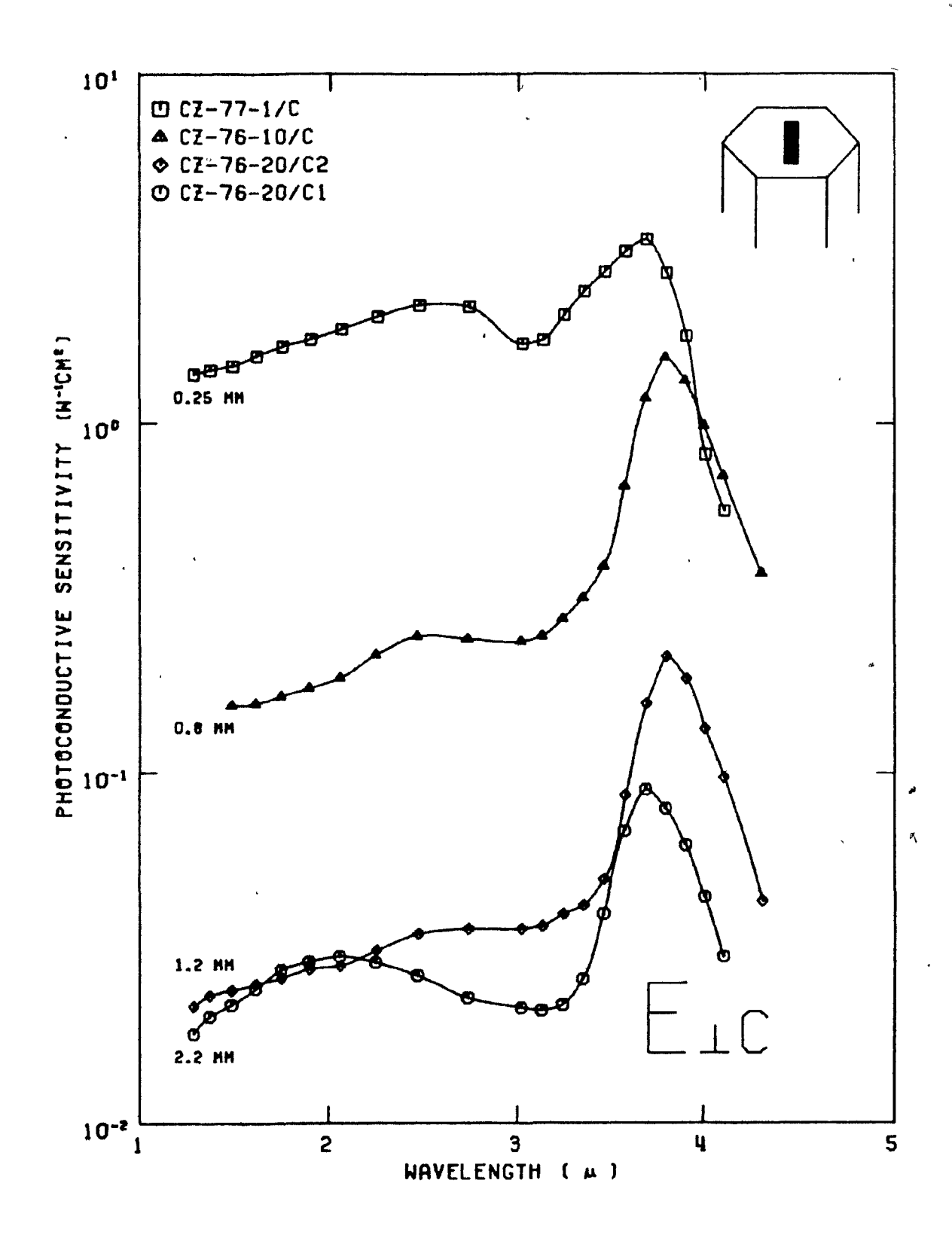


Fig. 5.6 Photoconductive sensitivity vs wavelength for sample orientation 'C' with Eic.

()

به باد در دید سده بید ب

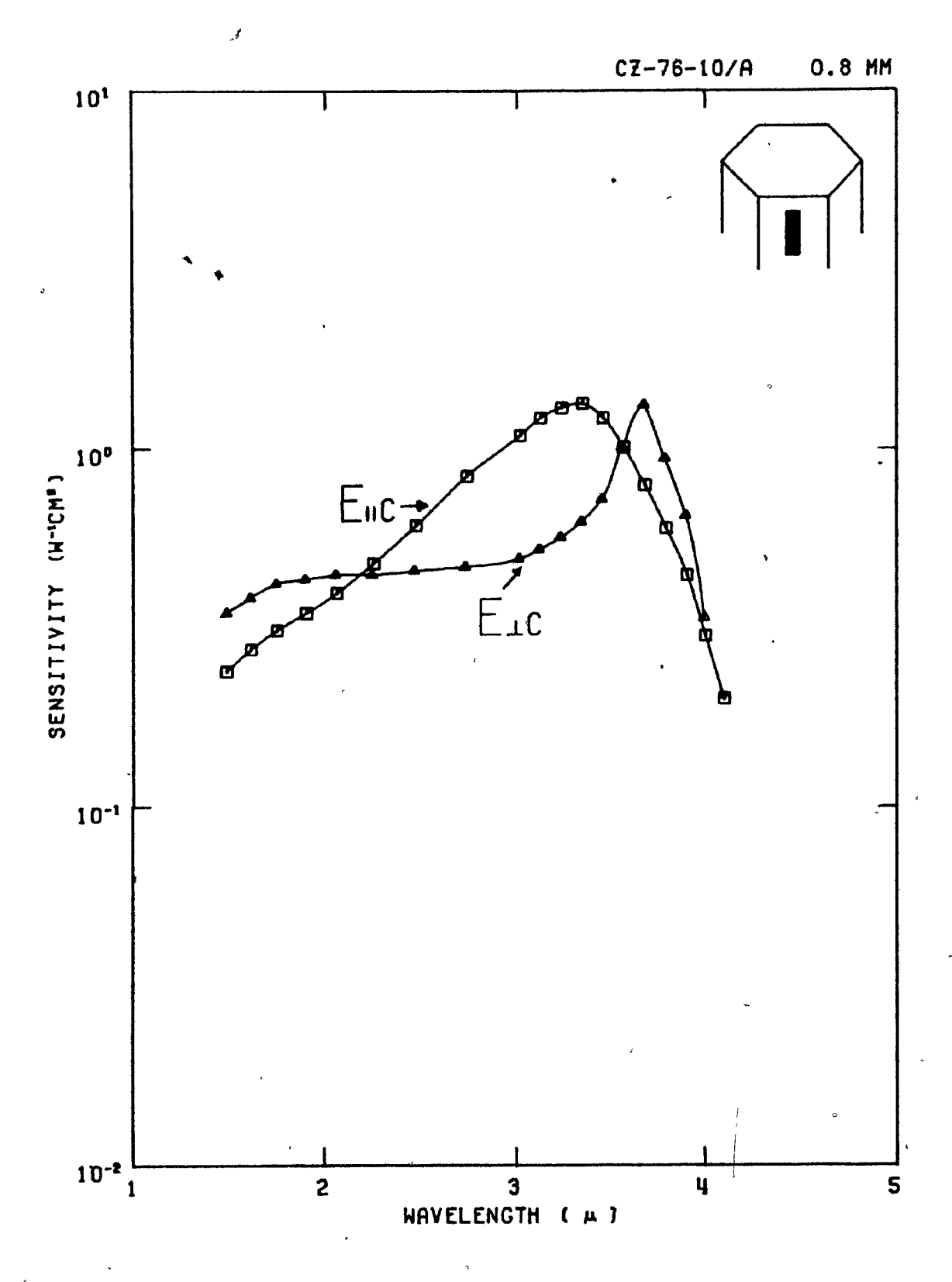
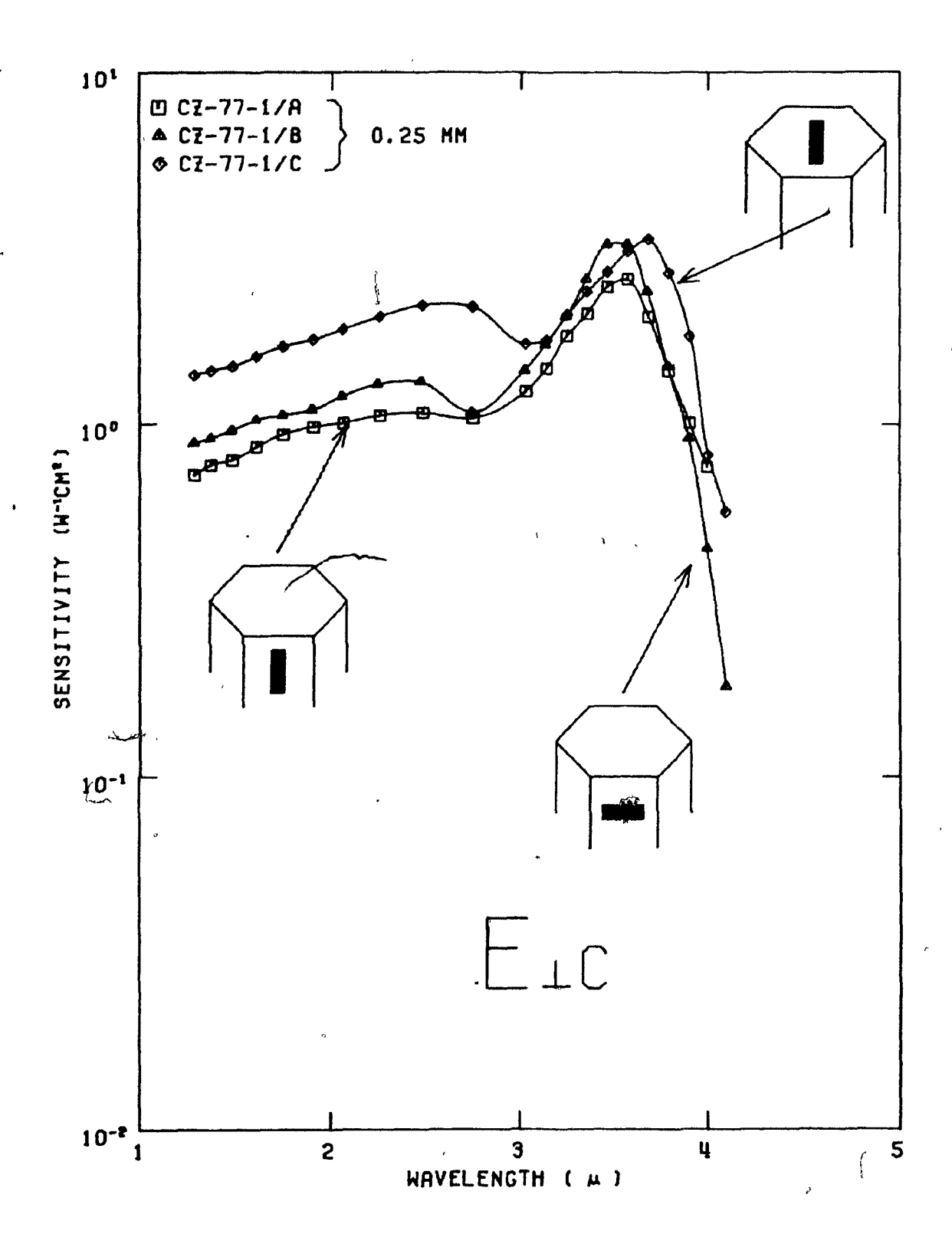
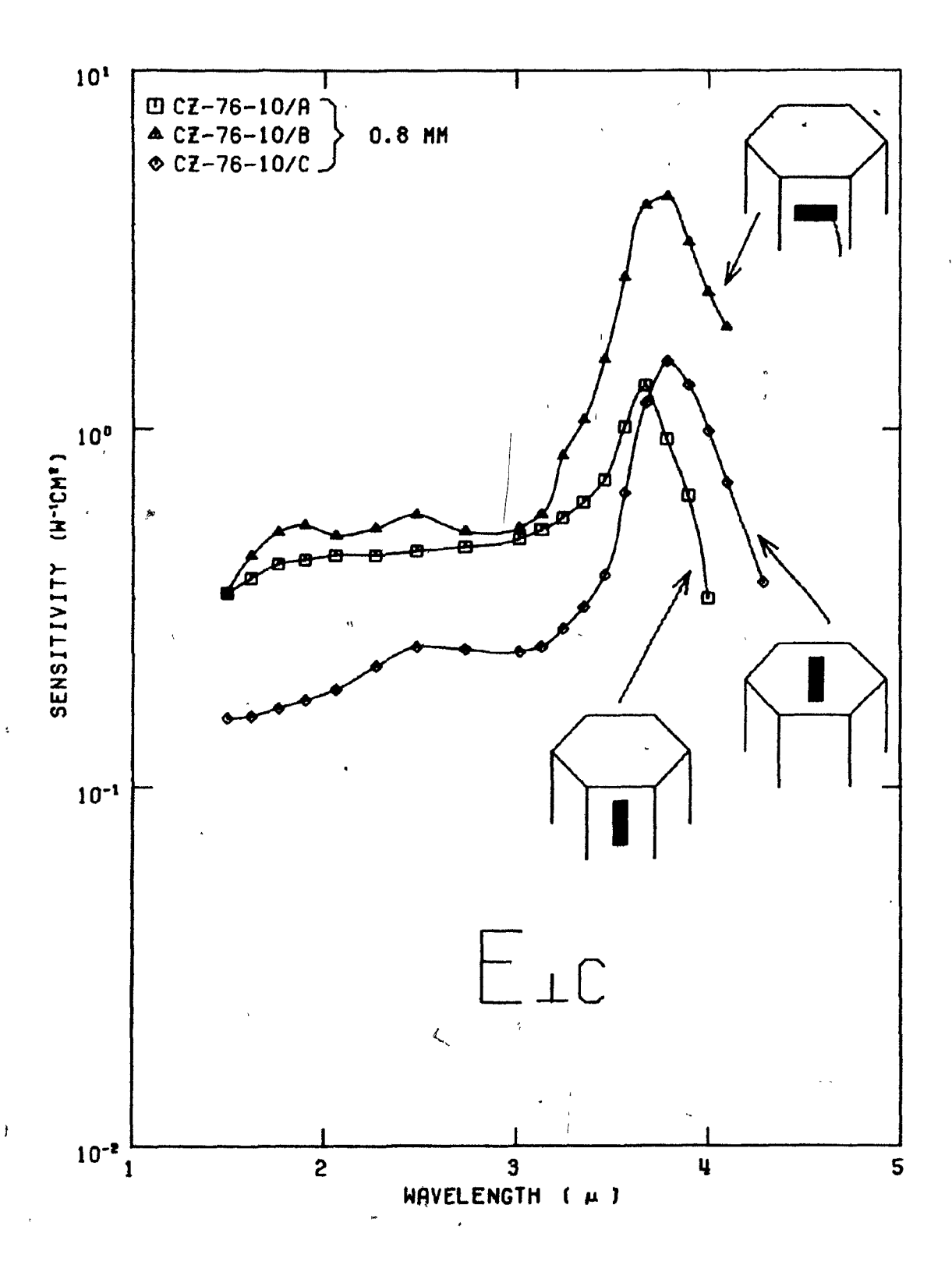


Fig. 5.7 Photoconductive sensitivity vs wavelength for the sample CZ-76-10/A.

,



Photoconductive sensitivity vs wavelength Fig. 5.8 for the three sample orientations with ${\tt E\botc.}$ (thickness = 0.25mm)



Photoconductive sensitivity vs wavelength Fig. 5.9 for the three sample orientations with $\mathtt{E} \bot \mathtt{c}$. (thickness = 0.8mm)

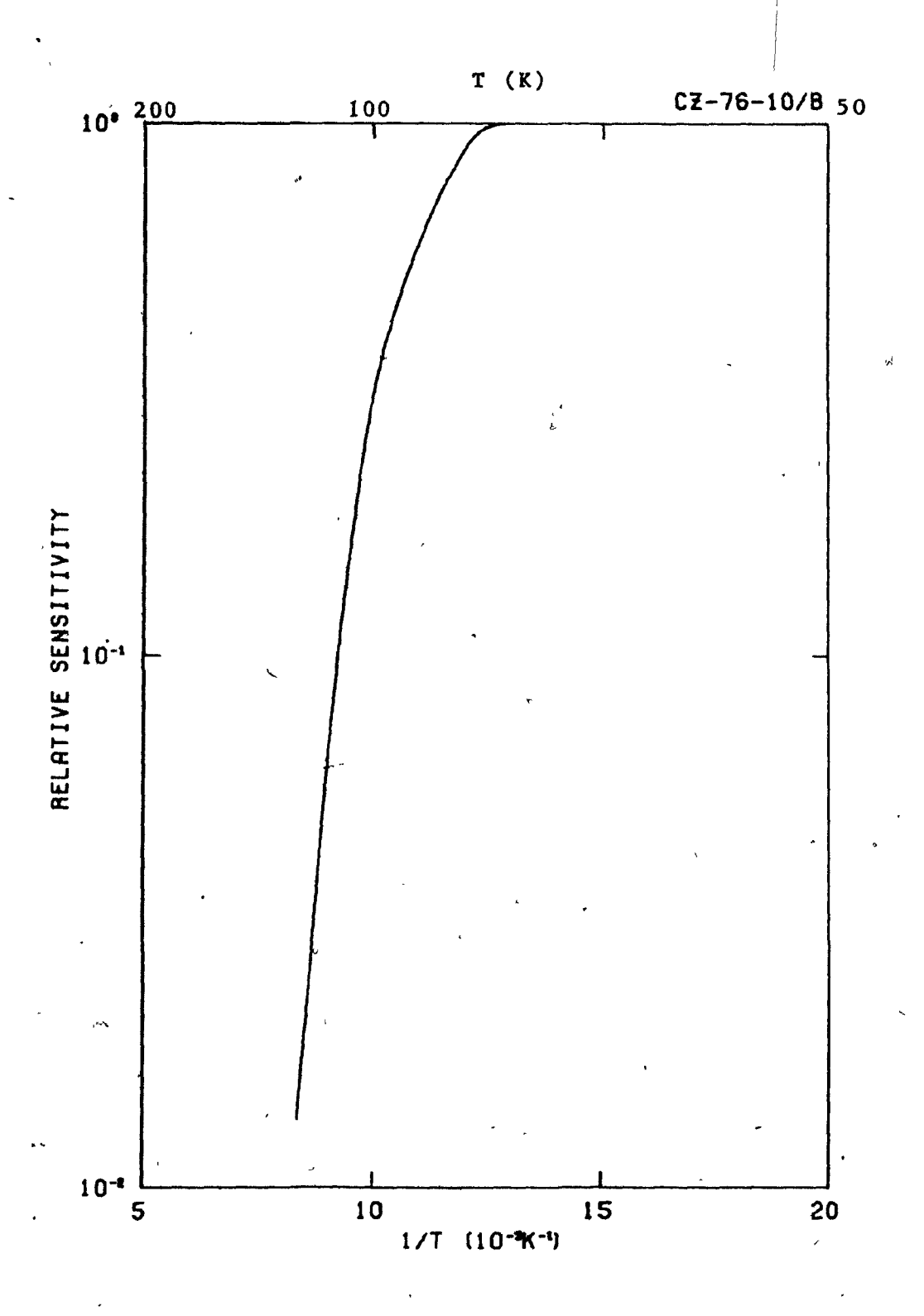


Fig. 5.10 Relative sensitivity vs reciprocal temperature for sample CZ-76-10/B at 3.6 microns.

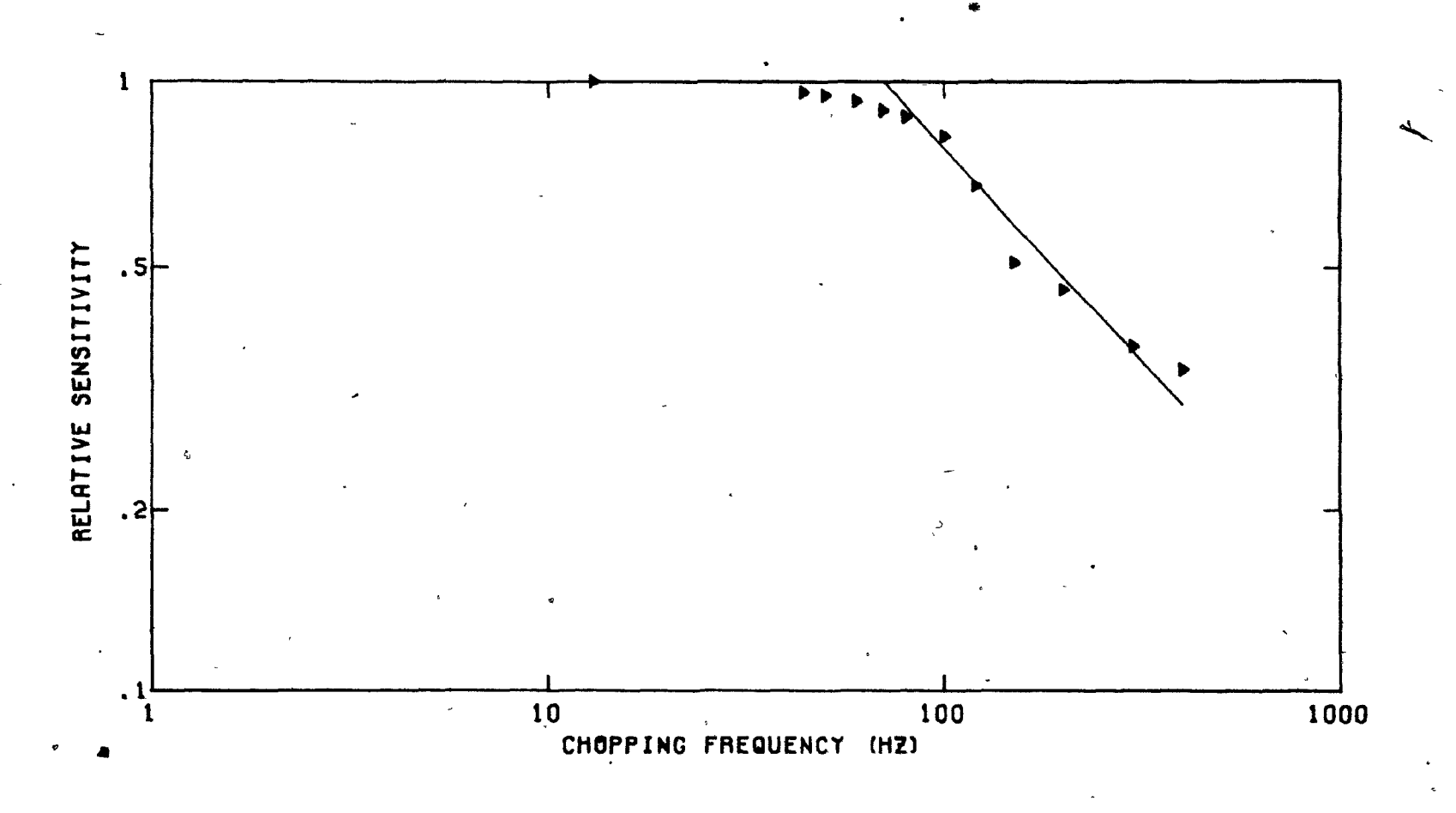


Fig. 5.11 Relative sensitivity vs chopping frequency for sample CZ-76-10/B at 3.6 microns, 77 K.

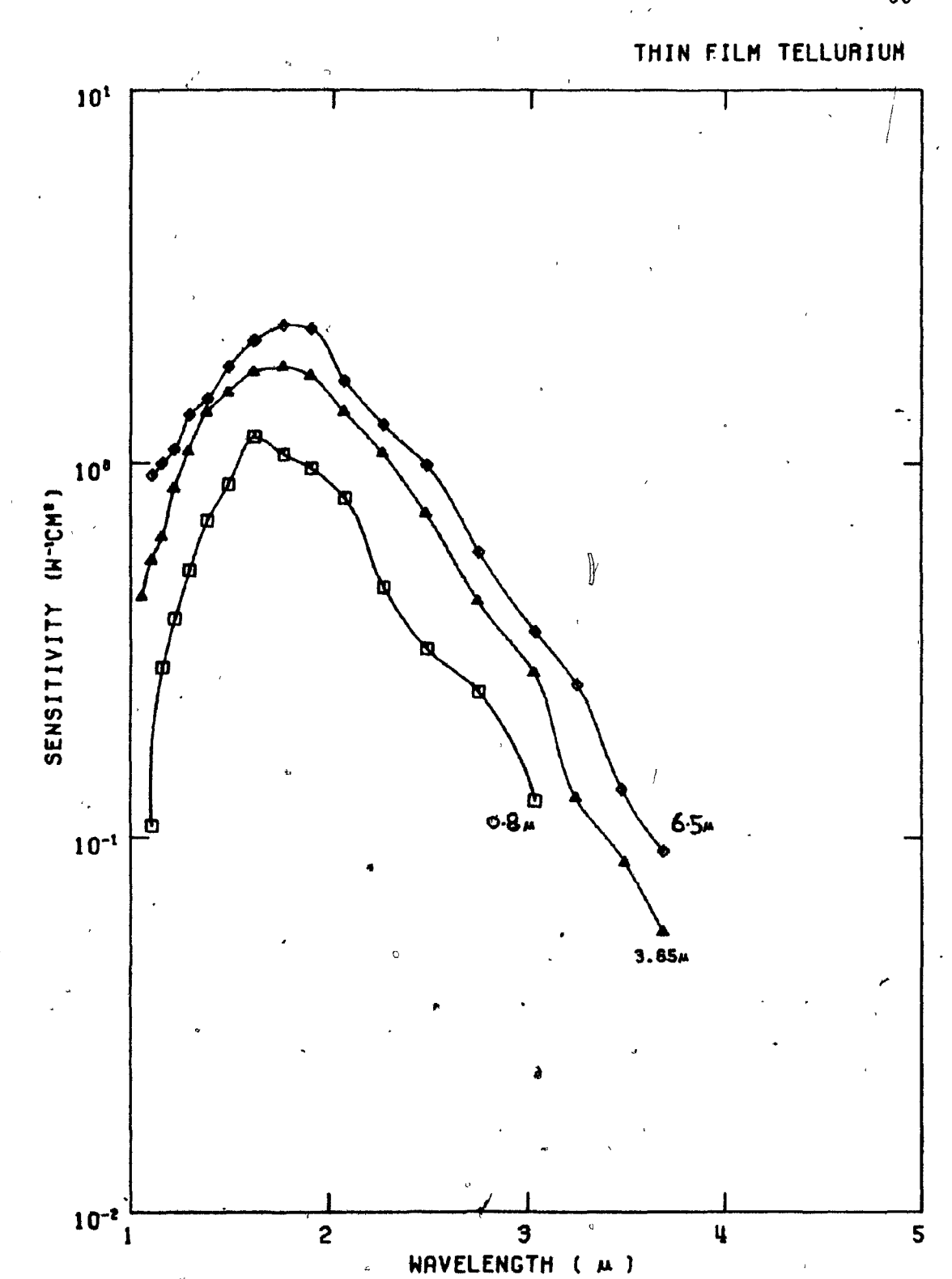


Fig. 5.12 Photoconductive sensitivity vs wavelength for the three thin film polycrystalline samples at 77 K.

CHAPTER VI

INTERPRETATION OF RESULTS

The results given in Chapter V are now examined in respect of the dependence of photoconductivity on sample thickness and wavelength. Arising from this, calculations are presented for surface recombination velocity and absorption coefficient.

6.1 Thickness Dependence

A log-log plot of the photoconductive sensitivity at a fixed wavelength of 2 microns against thickness for the various samples is shown in Fig. 6.1. The data shown can be divided into two groups, one for the thin film polycrystalline samples and the other for those in bulk single crystal form. Major differences between the two groups are evident.

The bulk single crystal samples show an increasing sensitivity for a decreasing thickness. A straight line of slope -1 drawn through the points is approximately consistent with the general trend of the results. This indicates an approximate variation of sensitivity as inverse thickness, ie. $\Delta\sigma/\sigma_0 \ll 1/d$, as expected from equation (2.3) of Chapter II.

The thin film samples on the other hand show an increasing sensitivity with increasing thickness. According to 4 the simple treatment presented in Chapter II,

equation (2.11) for example, one expects the sensitivity to be independent of the thickness for thin samples. However, referring to equation (2.22) of the more exact treatment of photoconductivity, in which the surface recombination velocity s is nonzero, it can be shown that for small thicknesses there is an increase in sensitivity with increase in thickness. Physically, this can be explained as follows. The recombination at the surface is faster than in the bulk of the sample and hence the excess concentration near the surface is lower. As the sample thickness is increased this lower concentration layer occupies a smaller fraction οf the sample, so that the average conductivity increases. It should be noted, however, that if the incident surface, no increase of conductivity with sample thickness would occur.

From Fig. 6.1 it would appear that the optimum sample thickness for achieving maximum photoconductive sensitivity is of the order of 0.1 mm.

6.2 Surface Recombination Velocity for Bulk Samples

In order to interpret the results of the photoconductivity measurements according to the theory presented in Sec. 2.3, it is convenient to express the results in terms of photon sensitivity, defined as $\Delta O/(O_0 J)$. This quantity is the relative change of conductivity per unit incident photon flux $(J=J_e/h^{\nu})$ and is plotted against wavelength for the various bulk samples in Figs. 6.2 - 6.6.

noted the peak of photon sensitivity is generally followed in each case by a long tail as the wavelength of illumination is decreased. Superimposed on this decrease are undulations, which will not be considered for the present. The general decrease conforms to the theory presented in Chapter II, where it was shown that with increase in the, value of absorption coefficient (corresponding to a decrease of wavelength), the sensitivity beyond the maximum decreases towards a constant value. Accordingly, the ratio $\Delta P_{co} / \Delta P_{max}$ was obtained from the ratio of the 'plateau' to the maximum sensitivity for a particular sample from the corresponding plot in Fig. 6.2 - 6.6 By using the curve in Figs. 2.3 - 2.6 with the appropriate d/L value for this sample, the value of K was determined. recombination velocity s was then calculated from the formula $A = s \mathcal{T}/L$. The diffusion length L employed in this expression was found using the relation L = $\sqrt{D^{\gamma}}$ = $\sqrt{kT\mu_{n}\gamma/e}$ = $3.64 ext{ } 10^{-2} ext{ cm, with an assumed lifetime of } 10^{-4} ext{ sec}$ and an electron mobility of 2000 cm2volt-1sec-1. Values of s were determined in this way for all the samples and the averaged results for each sample are listed in Table III.

It is noted here that there is a considerable spread of the average values from about 1200 cm/sec to 5300 cm/sec. While Grosse and Winzer reported a higher s value for the (0001) plane compared with the (1010) surface, this is not evident from the results presented in Table III.

6.3 Absorption Coefficient

The absorption coefficient K of the samples as a function of wavelength was calculated from the plots of Fig. 6.2 to Fig. 6.6 in the following way. For a given sample the ratio $\Delta P/\Delta P_{max}$ at a certain wavelength was obtained from the appropriate photon sensitivity plot. Then the value of Kd corresponding to this ratio was read off the curve in Figs. 2.3 - 2.6 for the appropriate d/L ratio and & value. From the known thickness d, the value of K was found. This was repeated for other wavelengths until the complete wavelength range was covered. Fig. 6.7 shows the K values for the two polarisations (Ellc and Elc) of two samples cut in the 'A' and 'B' orientations (Fig. 3.1). The photon sensitivity plots of these samples are given in Figs. 6.8 § 6.9.

For comparison the results of Blakemore & Nomura are also included in Fig. 6.7. It is noted that there is a clear difference between the variation of K. with wavelength for the two polarisations.

.

and a state of the state of the

سدند سان دار

TABLE III

Calculated Surface Recombination Velocities

Sample no.	Surface	Thickness (mm)	s (cm/sec)
CZ-77-1/A	(1010)	0.25	2708
CZ-76-10/A		0.8	1476
CZ-76-20/A2		~1.2	1409
CZ-76-20/A1		2.2	1653
CZ-77-1/B	(10 1 0)	0.25	2298
CZ-76-10/B		0.8	5300
CZ-76-20/B2		1.2	2553
CZ-76-20/B1		2.2	2870
CZ-77-1/C	(0001)	0.25	2549
CZ-76-10/C		0.8	3816
CZ-76-20/C2		1.2	2551
CZ-76-20/C1		2.2	,1205

Fig. 6.1 Photoconductive sensitivity vs sample thickness at a wavelength of 2 microns measured at 77 K (Eic)

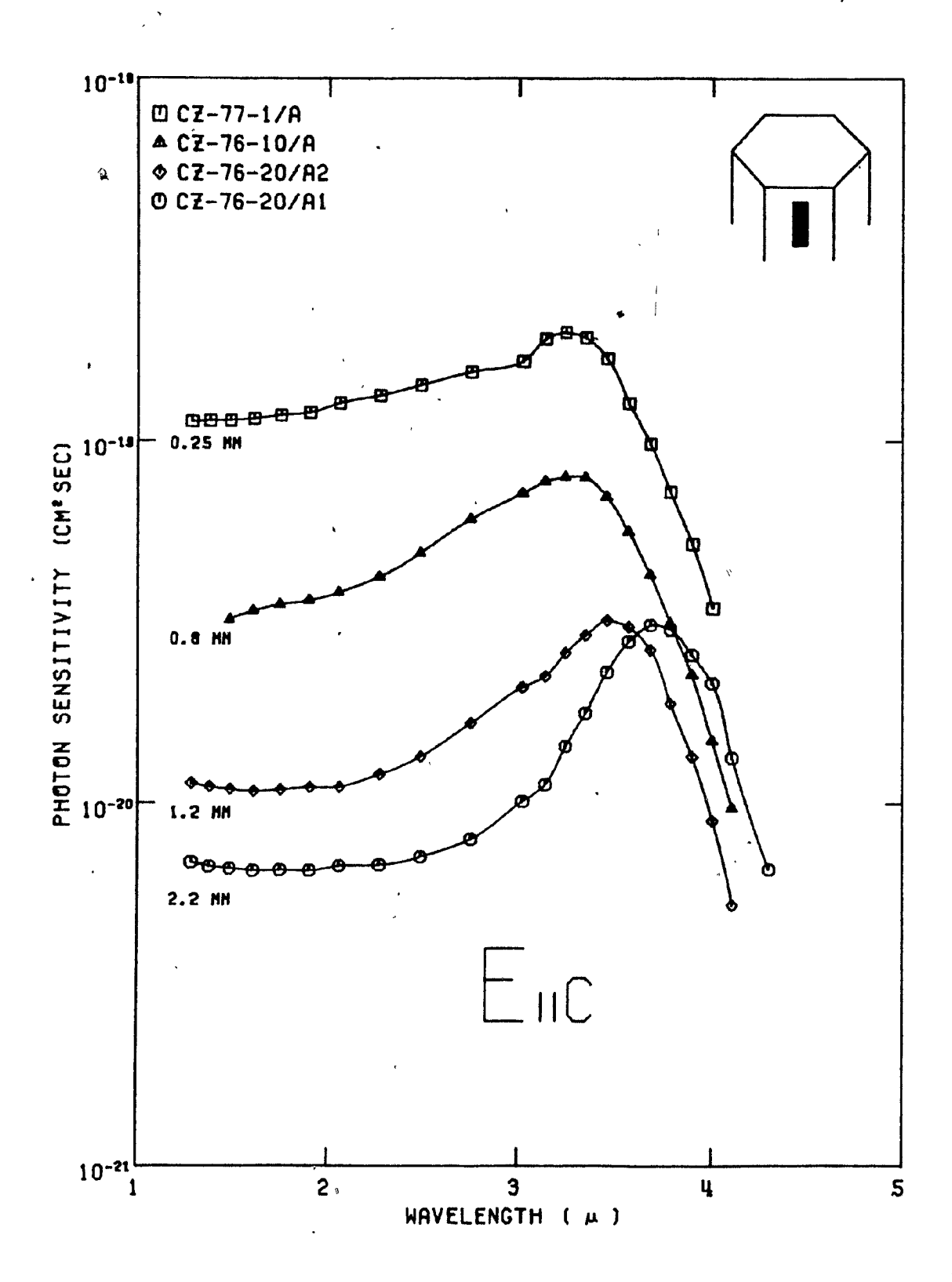


Fig. 6.2 Photon sensitivity vs wavelength for sample orientation 'A' with Ellc.

€

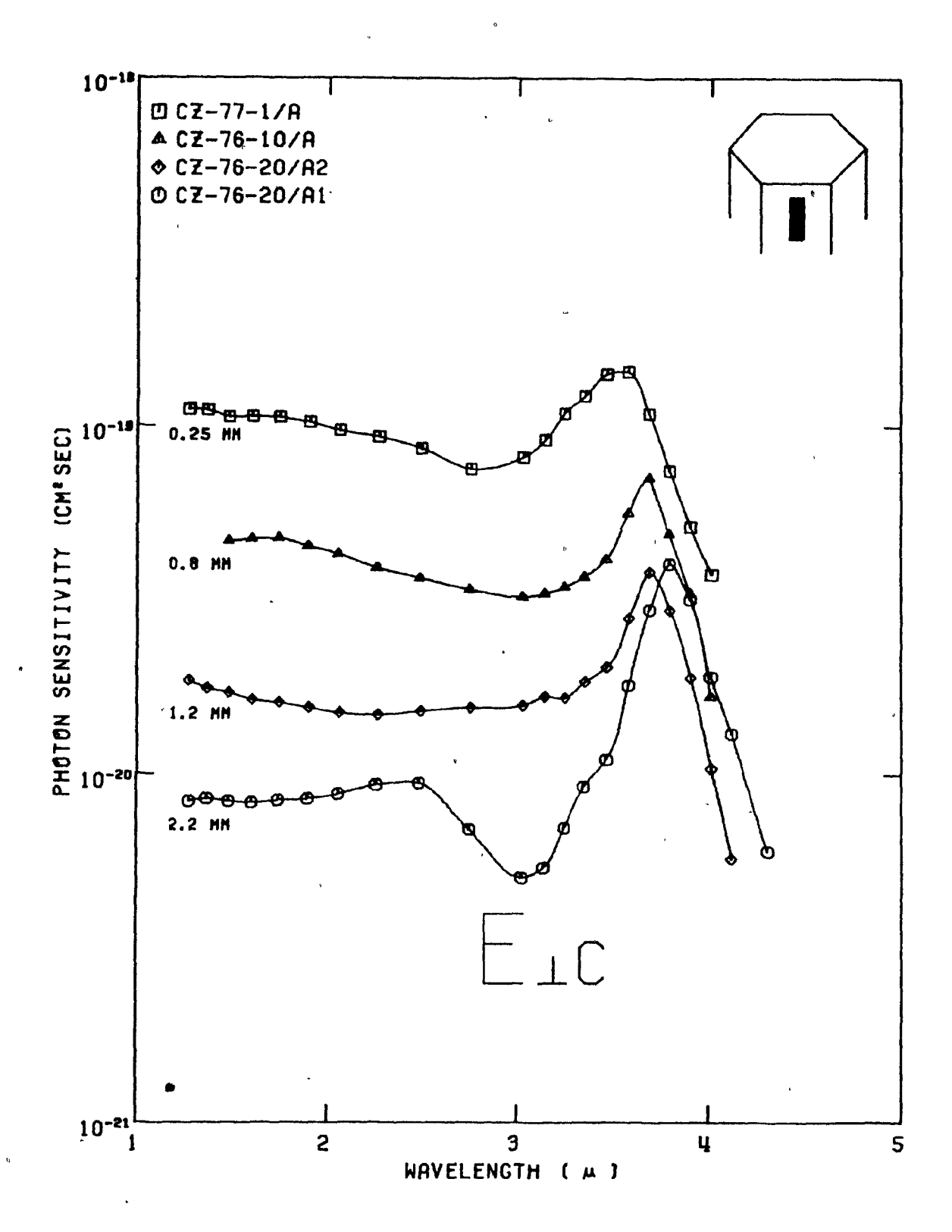


Fig. 6.3 Photon sensitivity vs wavelength for sample orientation 'A' with E \perp c.

1

*

100

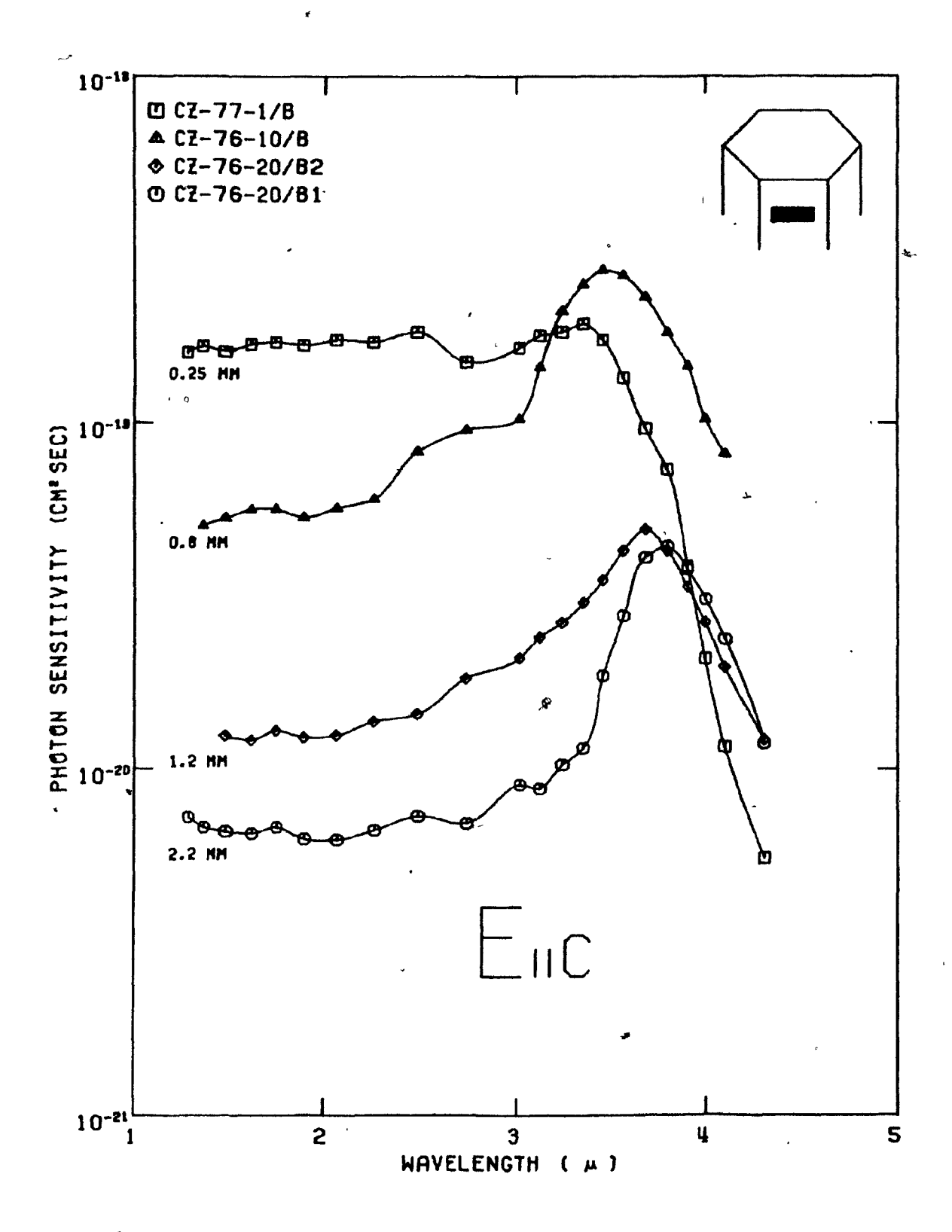


Fig. 6.4 Photon sensitivity vs wavelength for sample orientation 'B' with Elic.

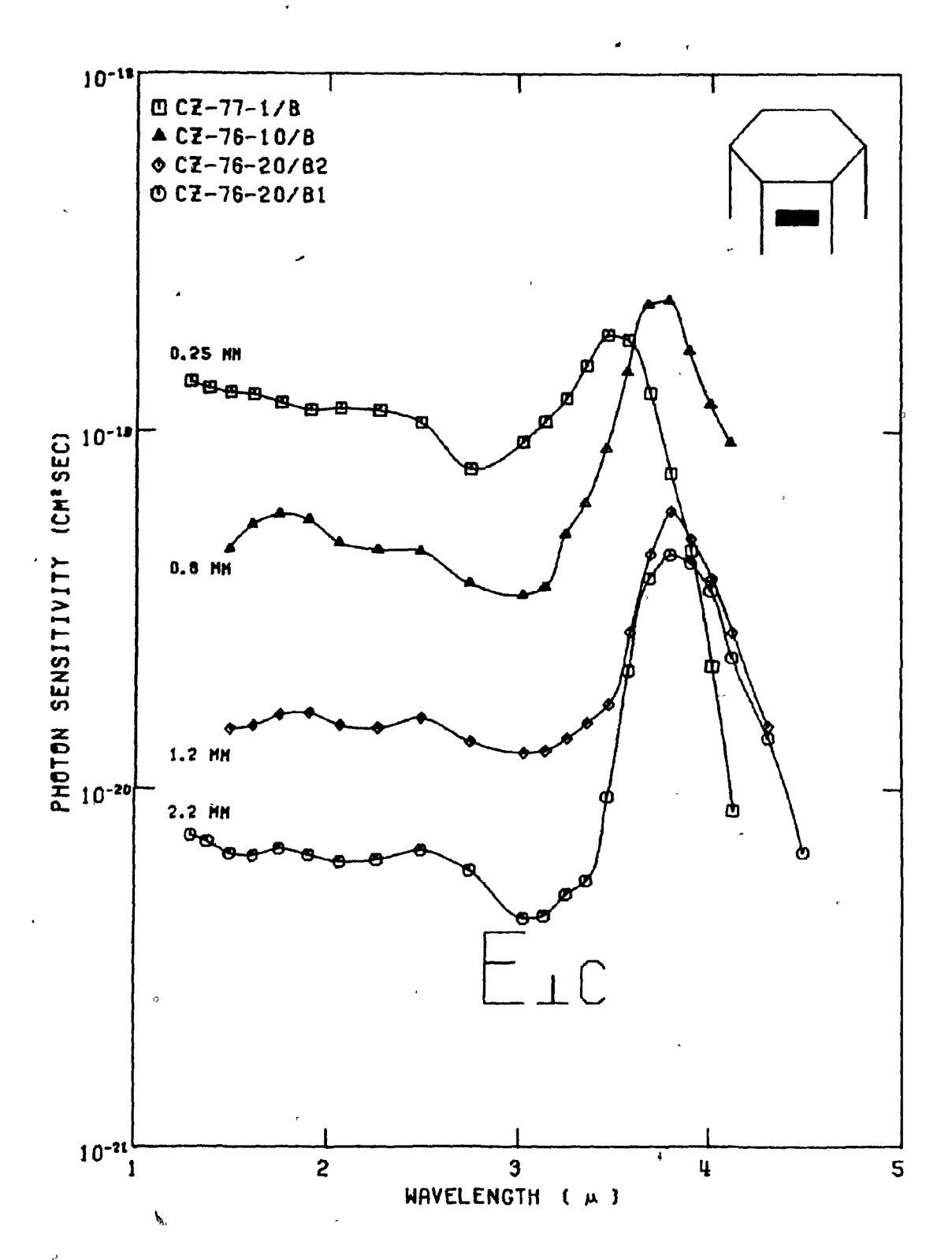


Fig. 6.5 Photon sensitivity vs wavelength for sample orientation 'B' with ELc.

O

e Theosphale s**ell**ateral parties on the home of the second of the sellateral second of the second o

و ر هوه جوددد

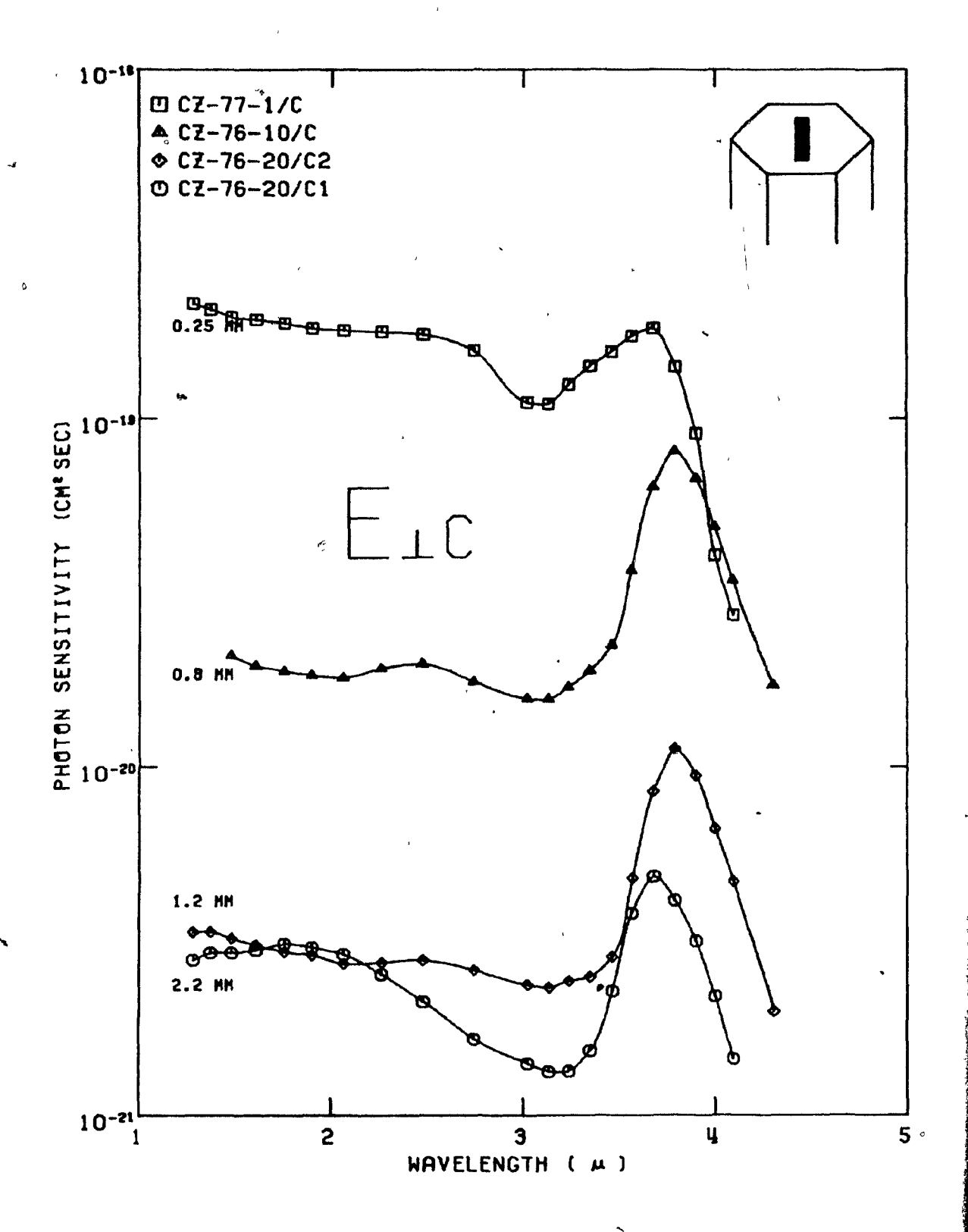


Fig. 6.6 Photon sensitivity vs wavelength for sample orientation 'C' with Elc.

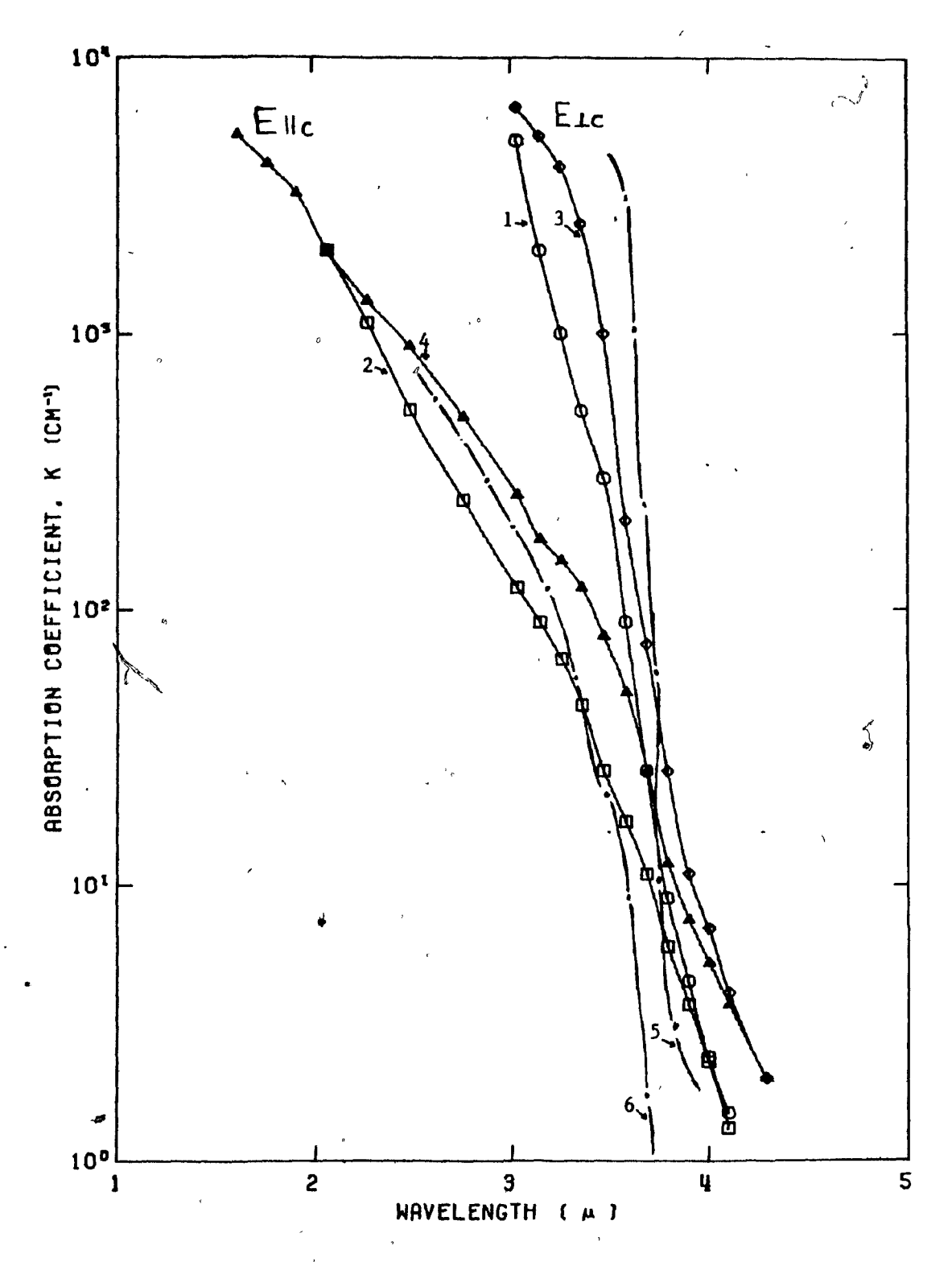


Fig. 6.7 Absorption coefficient vs wavelength. 3,4 - CZ-76-20/B2. 1,2 - CZ-76-20/A2 - Blakemore & Nomura 9.

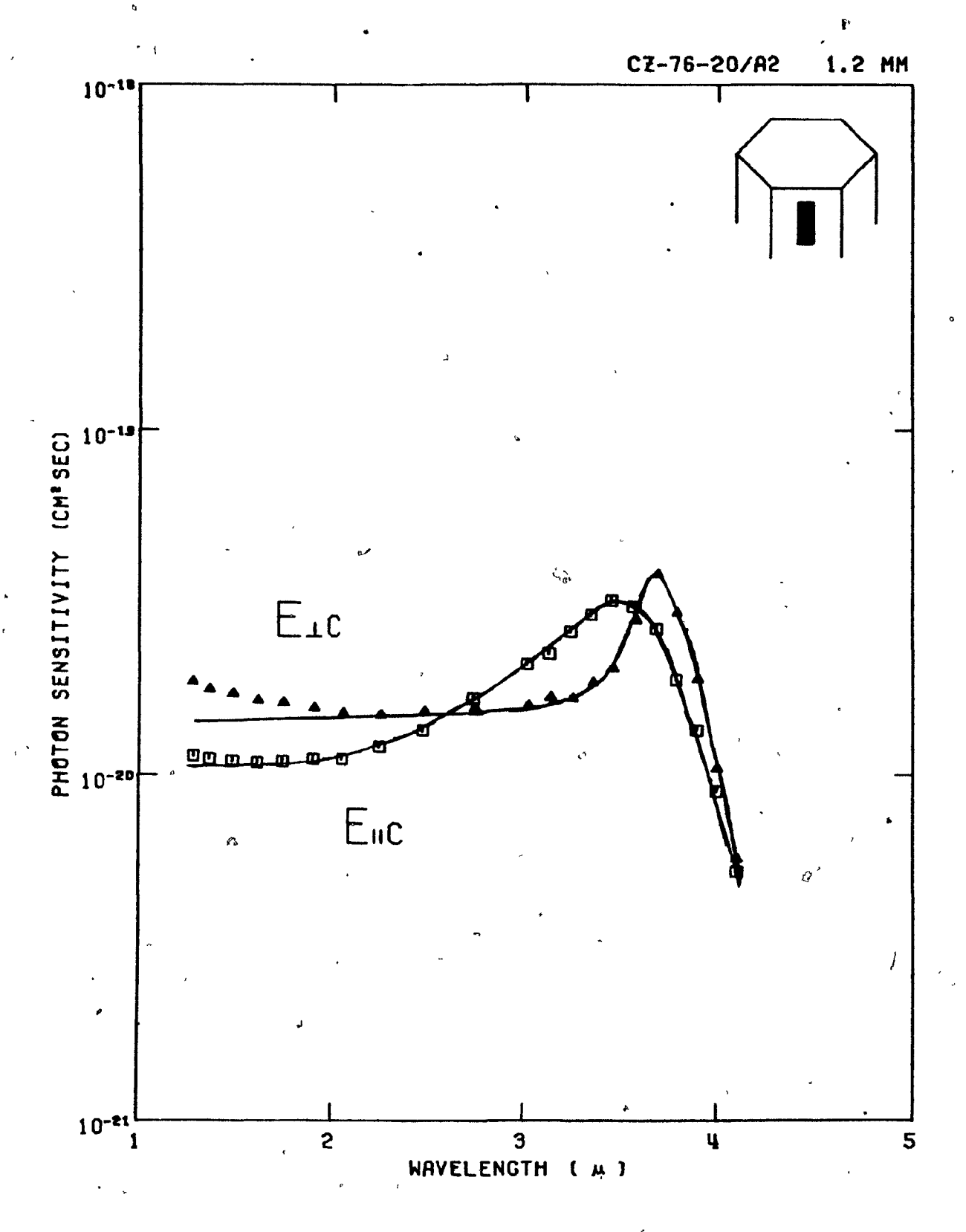


Fig. 6.8 Photon sensitivity vs wavelength for the sample CZ-76-20/A2.

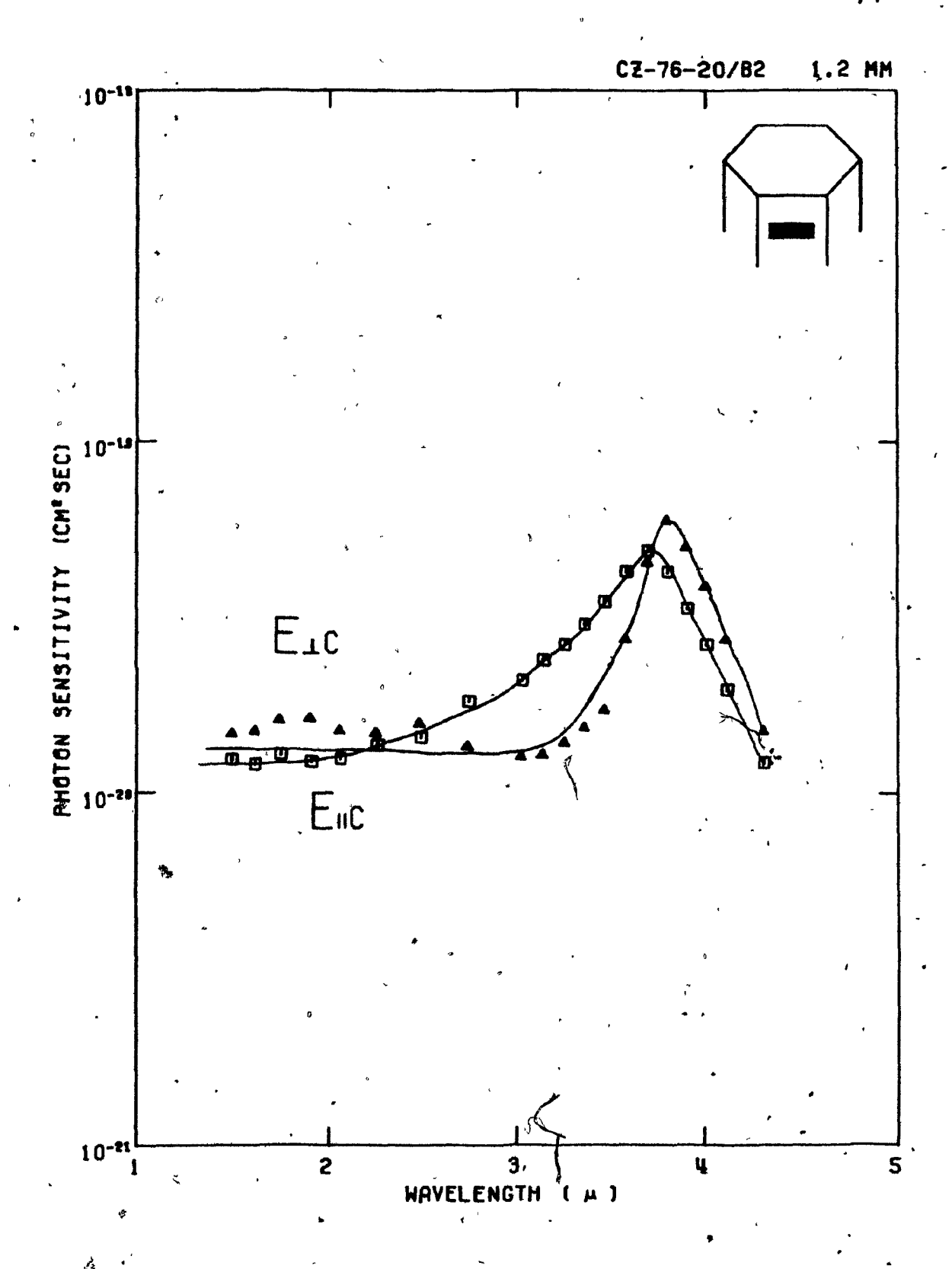


Fig. 6.9 Photon sensitivity vs wavelength for the sample CZ-76-20/B2.

>

CHAPTER VII

DISCUSSION AND CONCLUSIONS

The significance of the results and the conclusions drawn from them together with a discussion of apparatus shortcomings and associated errors are now presented.

7.1 Discussion *

It was shown in Chapter II that the photoconductive sensitivity is greatly influenced by the surface recombination velocity s. The rather large scatter in the results from one sample to another suggests a wide variation in surface conditions. The sensitivity to sample preparation has also been demonstrated elsewhere 7.10 by re-etching the sample surface, resulting in a generally increased photoconductivity.

Since the (0001) surface has dangling covalent bonds, whereas the (1010) face does not, one might expect the surface recombination velocity to be higher for the former planes. This was indeed reported by Grosse & Winzer but was not confirmed in the present work. However, their samples were cut abrasively with a wire saw and subsequently etched in hot concentrated sulfusic acid, while ours were chemically cut and polished without any abrasive treatment at all. Nevertheless, it is possible in the present work that a layer of oxide was left behind by the chemical treatment which could lead to enhanced s-values. Regarding

the values of s in Table III, it should be recalled that these were calculated assuming a lifetime of 0^{-4} sec. While the use of a smaller value of 7 hardly affects these values, a larger lifetime would reduce them.

The undulations of the photoconductive sensitivity is Loferski⁵ observed only one secondary next. maximum at 3.24 microns (for both ENc and E1c) and believed that it arose from the fundamental band structure of tellurium. Grosse & Winzer on the other hand have observed secondary maxima and minima attributed to interference in a 'Beilby layer' of disturbed or damaged tellurium some 1 to 2 microns thick. They also found that the minima (maxima) for Ellc coincided with the maxima (minima) for Elc. These undulations disappeared, at least for Elc, after etching in hot concentrated sulfuric acid. In the present work such a coincidence has not been observed. A more likely cause of the undulations, in the writer's opinion, is atmospheric absorption. As seen in Fig. 4.2 the distance travelled by the monochromatic beam of light to the tellurium sample is longer than that to the thermocouple detector. Therefore, in the presence atmospheric absorption at certain wavelengths, less energy reaches the tellurium sample than the thermocouple detector. consequently. reduces the measured photoconductive sensitivity, since the energy flux at the sample surface is estimated from the energy incident on the thermocouple, The fact that the measured incident energy at the detector also showed undulations at about the same wavelengths adds strength to thes hypothesis.

In addition to the sources of error described above, there are others which should be pointed out. Due to the relatively low energy output, especially at longer wavelengths, of the monochromator arising from the Nernst glower, it was necessary to have a fairly wide slit width of 0.25 mm in order to obtain a measurable photoconductivity. This slit width corresponds to a band width of 0.2 microns. Thus any fine structure in the spectral distribution would not be resolved.

17

In measuring photoconductivity, care was taken to avoid illuminating the end contacts to the sample. As a result of this photoconduction was restricted to only about 80% of the length of the sample. Consideration shows that due to this the sensitivity plotted in Figs. 5.2-5.6 should be increased by about 15 to 20 %. In addition there would be a difference in transmission between the window of the thermocouple detector (KBr) and that of the tellurium sample (IRTRAN-2). The reflection loss of about 45% at the tellurium surface also needs to be considered if one wants to calculate the absolute sensitivity to absorbed radiation. However, these various corrections have not been applied, since the calculations of s and K involve only relative changes of sensitivity.

The absorption coefficient, as calculated in Chapter VI follows the general trend reported by Blakemore & Nomura in that curves for Elc are much steeper than those for Elc. This confirms the general belief that the transition for Elc is direct. The present absorption coefficients extend to

lower wavelengths than those of Blakemore & Nomura and differ from them somewhat in absolute magnitude. It is seen, in any case, that photoconductivity measurements can be used to calculate absorption coefficients, accurately in the wavelength range where transmission measurements are extremely difficult due to the strong absorption.

The measured detectivity $D^* = Qf 2x10^8 \text{ cmHz}^{\frac{1}{2}} \text{watt}^{-1}$ at 23 Hz given in Chapter V is only a very conservative estimate of the actual value. It should be pointed out that one would have to study the variation of noise with bias current, chopping frequency, etc., to obtain an optimal operating point with the best noise performance. Since this preliminary study, such noise characteristics were not measured. In any case, during the photoconductive measurements, most of the % oise observed originated from sources external to the sample. Edwards, Butter and McGlauchlin11 have reported a tellurium device of 2.2×10^{11} cmHz $\frac{1}{2}$ watt -1detectivity background limited noise conditions at a frequency of 900 Hz. While this value is some three orders of magnitude higher than our estimated figure above, the difference can be roughly accounted for by the difference of the two the semiconductor frequencies, since decreases approximately as the reciprocal of the frequency.

Leaving noise considerations aside, the sensitivity between 2 and 3.5 microns is greater for ENC than for ELC and thus it would appear that this is the preferred orientation from a device point of view. Fig. 6.1 suggests a

maximum sensitivty for a sample thickness of 0.1 mm and hence an optimum device configuration would be a tellurium crystal some 100 microns thick with the (1010) plane exposed to the incident radiation.

7.2 Summary of Conclusions

It is convenient to summarize the conclusions of the present study as follows.

Bulk monocrystalline tellurium samples

- 1) The spectral distribution of photoconductivity was confirmed to have the main features reported previously⁷, namely a maximum at a longer wavelength for Eic than for Eic and also a correspondingly steeper decrease with decreasing wavelength. Thus for Eic the photoconductivity is larger than for Eic between 2 and 3.5 microns.
- 2) The photoconductive sensitivity at 77 K was found to increase with decreasing sample thickness approximately in accordance with theory.
- 3) No dependence of photoconductivity on the crystalline orientatation of the sample was found.
- 4) A difference of surface recombination velocity between the (0001) and (1010) surfaces was not confirmed. The magnitudes ranged from about 1000 to 5000 cm/sec.
- 5) Absorption coefficient values calculated from the results extended to lower wavelengths than those previously reported from transmission measurements 9.

Polycrystalline thin film samples

- 6) In the thin film polycrystalline samples, the photoconductivity increased with increase of sample
 thickness. The photoconductivity maximum was displaced
 to shorter wavelengths compared with the bulk samples.
- 7) An optimal sample thickness for maximum photo-

7.3 Future Work

A great deal of further work is needed on tellurium photoconductivity both from a scientific and a device point of view. Some suggestions for future work on this topic are listed below.

- 1) Samples with side arms should be used to eliminate any effect of the contacts.
- 2) Experiments on samples prepared with different surface treatments should be conducted to achieve a consistent value of s.
- 3) Energy incident on the sample should be measured by a calibrated detector placed in the sample plane. Thus effect of atmospheric absorption could be eliminated.
- 4) Photoconductivity measurements should be made at different temperatures.
- 5) Lifetime measurements should be made on the samples to accurately relate theory to the experimental results.
- biasing committions, and frequency should be made.
- 7) Attempts should be made to grow monocrystalline thin film tellurium on a substrate.

REFERENCES

- [1] J.S.Blakemore, D.Long, K.C.Nomura and A.Nussbaum in "Progress in Semiconductors", John Wiley & Sons, New York, 1962, Vol. 6
- [2] D.F.Edwards and M.Mercado, "Ultimate Sensitivity and Practical Performance of the Tellurium Photoconductive Detector", Infrared Phys., 1, 17(1961)
- [3] I. Shih and C.H. Champness, "Czochralski Growth of Tellurium Single Crystals", Journal of Crystal Growth,
 44, 492(1978)
- T.S.Moss, "Infrared Photoconductivity in Layers of Tellurium and Arsenic", Proc. Phys. Soc., London,
 A62, 264(1949)
- [5] J.J.Loferski, "Infrared Optical Properties of Single Crystals of Tellurium", Phys. Rev., 93, 707 (1954)
- [6] V.A.Vis, "Photoconductivity in Single Crystal Tellurium", J. Appl. Phys., 35, 360 (1964)
- [7] F.Grosse and K.Winzer, "Photoleitungs- und Lebensdauermessungen an Tellur", Phys. Stat. Sol. 13, 269 (1966)

- [8] M.El-Azab, C.McLaughlin and C.H.Champness,
 "Preparation and Characterization of Tellurium
 Surfaces", Journal of Crystal Growth, 28, 1(1975)
- [9] J.S.Blakemore and K.C.Nomura, "Intrinsic Optical Absorption in Tellurium", Phys. Rev., 127, 1024(1962)
- [10] I.Shih (private communication)
- [11] D.F.Edwards, C.D.Butter, L.D.McGlauchlin, "Photoconductivity in Single Crystal Tellurium", Institute of Science and Technology, University of Michigan, Ann Arbor, Michigan, March 1961.

APPENDIX A

It is required to solve the differential equation

$$L^{2}\frac{d^{2}\Delta p}{dy^{2}} - \Delta p = -JKT \exp(-Ky)$$
 (A.1)

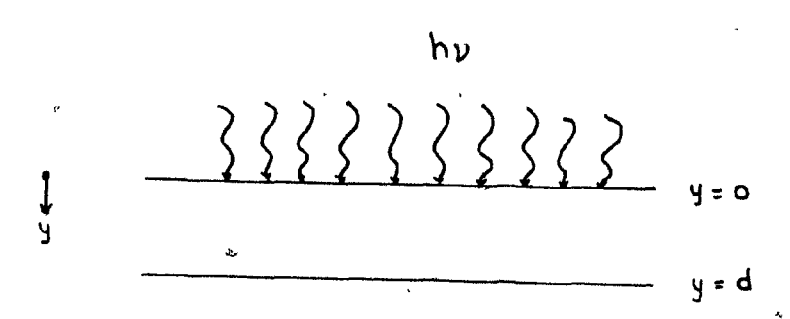


Fig. A.1

In regard to the situation in Fig. A.1, where the sample is assumed to be infinitely long, the solution is,

$$\Delta p = A \cosh \frac{y}{L} + B \sinh \frac{y}{L} + \frac{JK\Upsilon}{1 - K^2L^2}$$
 (A.2)

This is verified as follows:

$$\frac{d\Delta p}{dy} = \frac{A}{L} \sinh \frac{y}{L} + \frac{B}{L} \cosh \frac{y}{L} - \frac{JK\tau}{1 - K^2L^2} K \exp(-Ky)$$
(A.3)

$$\frac{d^{2}\Delta p}{dv^{2}} = \frac{A}{L^{2}} \cosh \frac{y}{L} + \frac{B}{L^{2}} \sinh \frac{y}{L} + \frac{JKY}{1 - K^{2}L^{2}} K^{2} \exp(-Ky)$$
 (A.4)

 $A.1xL^2 - A.2$ gives

$$L^{2}\frac{d^{2}\Delta p}{dy^{2}} - \Delta p = A \cosh \frac{y}{L} + B \sinh \frac{y}{L} + \frac{JK\tau}{1 - K^{2}L^{2}} K^{2}L^{2} \exp(-Ky)$$

$$- A \cosh \frac{y}{L} - B \sinh \frac{y}{L} - \frac{JK\tau}{1 - K^{2}L^{2}} \exp(-Ky)$$

$$= - JK\tau \exp(-Ky)$$

Hence the solution (A.2) is verified.

Boundary conditions:

The diffusion currents at the two surfaces (Fig. A.1) are given by:

i)
$$-D\frac{d\Delta p}{dy} = -\Delta p$$
 s at $y = 0$

ii)
$$-D\frac{d\Delta p}{dy} = \Delta p s$$
 at $y = d$

1)
$$-D\left[\frac{A}{L}\sinh\frac{y}{L} + \frac{B}{L}\cosh\frac{y}{L} - \frac{JK\tau}{1 - \kappa^2L^2}K\exp(-\kappa y)\right]$$

$$= -s \left[A \cosh \frac{y}{L} + B \sinh \frac{y}{L} + \frac{JK\tau}{1 - K^2L^2} \exp(-Ky)\right]$$

At
$$y = 0$$
,

$$-D\frac{B}{L} + D\frac{JKY}{1 - K^2L^2} K = -sA - s\frac{JKY}{1 - K^2L^2}$$

$$B = AA + (KL+\alpha) \frac{JK\gamma}{1 - K^2L^2} \quad \text{where } A = \frac{sL}{D}$$

11)
$$-D \frac{d\Delta p}{dv} = \Delta p s$$
 at $y = d$

$$-D\left[\frac{A}{L}\sinh\frac{y}{L} + \frac{B}{L}\cosh\frac{y}{L} - \frac{JK\Upsilon}{1 - K^2L^2}K^{\circ}\exp(-Ky)\right]$$

= s[A cosh
$$\frac{y}{L}$$
 + B sinh $\frac{y}{L}$ + $\frac{JK\zeta}{1 - K^2L^2}$ exp(-Ky)]

At y = d,

$$A[s cosh^{-+} - sinh^{-}] + B[s sinh^{-+} - cosh^{-}] = (DK - s) \frac{JK^{+}}{1 - K^{2}L^{2}} exp(-Kd)$$

Multiplying both sides of the above equation by $\frac{L}{D}$ & with $\alpha = \frac{sL}{D}$,

Substituting B = $dA + (KL+\infty) \frac{JKT}{1 - K^2L^2}$, we get

 $A[x^{2}\sinh_{-}^{d}+2x\cosh_{-}^{d}+\sinh_{-}^{d}] = \frac{JK\tau}{1-K^{2}L^{2}}[(KL-x)\exp(-Kd)-(KL+x)(A\sinh_{-}^{d}+\cosh_{-}^{d})]$

$$A = \frac{JK\tau}{\int_{1-K^2L^2}^{1-K^2L^2}} \frac{(KL-\alpha)\exp(-Kd) - (KL+\alpha)(\alpha \sinh + \cosh - 1)}{\int_{L}^{d} \int_{L}^{d}} \frac{d}{(\alpha \lambda^2 \sinh + 2\alpha \cosh + \sinh - 1)}$$

nd

$$B = \alpha A + (KL+\alpha) \frac{JK^{2}}{1-K^{2}L^{2}}$$

$$B = \frac{JK\tau}{1-K^2L^2} \frac{\alpha(KL-\alpha)\exp(-Kd) - \alpha(KL+\alpha)(\alpha(\sin nh^2 + \cosh^2 + \cos h^2))}{\frac{d}{1-K^2L^2}} + \frac{JK\tau}{1-K^2L^2}$$

$$(\alpha^2 \sin h^2 + 2\alpha(\cosh^2 + \sinh^2 + \cos h^2))$$

$$B = \frac{\int_{JK7}^{d} \left[\frac{d}{d(KL-d)\exp(-Kd) - d(KL+d)(d\sinh - +\cosh -)} \right]}{\int_{L}^{d} \frac{d}{dd} \frac{d}{dd}}$$

$$(d^{2}\sinh - +2d\cosh - +\sinh -)$$

$$L$$

$$+\frac{(KL+\alpha)(\alpha^{2}sinh-+2\alpha cosh-+sinh-)}{L} + \frac{d}{(\alpha^{2}sinh-+2\alpha cosh-+sinh-)}$$

$$L \qquad L \qquad L$$

$$L \qquad L \qquad L$$

$$B = \frac{JK?}{1-K^2L^2} \frac{\alpha(KL-\alpha)\exp(-Kd)+(KL+\alpha)(\alpha\cosh+sinh-)}{\frac{d}{L}} \frac{d}{\alpha^2\sinh-+2\alpha\cosh+sinh-)} L L L$$

$$\begin{split} & \Delta P = \int_{0}^{d} \Delta p \ dy = \int_{0}^{d} \left[A \cos \frac{y}{L} + B \sin \frac{y}{L} + \frac{y K t}{1 - K^{2} L^{2}} \exp(-Ky) \right] \ dy \\ & = A L \sin \frac{d}{L} + B L \left(\cosh \frac{d}{L} - 1 \right) + \frac{J^{2}}{1 - K^{2} L^{2}} \left[1 - \exp(-Kd) \right] \\ & = \frac{J^{2}}{1 - K^{2} L^{2}} X L \ \sinh \frac{d}{L} + \frac{d}{(k^{2} \sinh \frac{d}{L} + 2k \cosh \frac{d}{L} + 3 \sinh \frac{d}{L})}{(k^{2} \sinh \frac{d}{L} + 2k \cosh \frac{d}{L} + 3 \sinh \frac{d}{L})} \\ & + \frac{J^{2}}{1 - K^{2} L^{2}} K L \left(\cosh \frac{d}{L} - 1 \right) + \frac{d}{(k^{2} \sinh \frac{d}{L} + 2k \cosh \frac{d}{L} + 3 \sinh \frac{d}{L})}{(k^{2} \sinh \frac{d}{L} + 2k \cosh \frac{d}{L} + 3 \sinh \frac{d}{L})} \\ & + \frac{J^{2}}{1 - K^{2} L^{2}} \left[1 - \exp(-Kd) \right] \\ & \text{With } \sinh \frac{d}{L} = 2 \sinh \frac{d}{2L} \cosh \frac{d}{2L} \left(\cosh \frac{d}{L} \right) \left(\frac{d}{2k \sinh \frac{d}{L} + 2k \cosh \frac{d}{L} + 3 \sinh \frac{d}{L}} \right) \\ & + \frac{J^{2}}{1 - K^{2} L^{2}} K L \left(2 \sinh \frac{d}{2L} \right) \left(\frac{d}{2L} \cosh \frac{d}{L} \right) \left(\frac{d}{2k \sinh \frac{d}{L} + 2k \cosh \frac{d}{L} + 3 \sinh \frac{d}{L}} \right) \\ & + \frac{J^{2}}{1 - K^{2} L^{2}} X L \left(2 \sinh \frac{d}{2L} \right) \left(\frac{d}{2L} \left(\frac{d}{2k \sinh \frac{d}{L} + 2k \cosh \frac{d}{L} + 3 \sinh \frac{d}{L}} \right) \left(\frac{d}{2k \sinh \frac{d}{L} + 2k \cosh \frac{d}{L} + 3 \sinh \frac{d}{L}} \right) \\ & + \frac{J^{2}}{1 - K^{2} L^{2}} K L \left(2 \sinh \frac{d}{2L} \right) \left(\frac{d}{2k \sinh \frac{d}{L} + 2k \cosh \frac{d}{L} + 3 \sinh \frac{d}{L}} \right) \left(\frac{d}{2k \sinh \frac{d}{L} + 2k \cosh \frac{d}{L} + 3 \sinh \frac{d}{L}} \right) \left(\frac{d}{2k \sinh \frac{d}{L} + 2k \cosh \frac{d}{L}} \right) \left(\frac{d}{2k \sinh \frac{d}{L} + 2k \cosh \frac{d}{L}} \right) \left(\frac{d}{2k \sinh \frac{d}{L} + 2k \cosh \frac{d}{L}} \right) \left(\frac{d}{2k \sinh \frac{d}{L} + 2k \cosh \frac{d}{L}} \right) \left(\frac{d}{2k \sinh \frac{d}{L}} \right) \left(\frac{d}{2k \cosh \frac{d}{L}} \right) \left(\frac{d}{2k \sinh \frac{d}{L}} \right) \left(\frac{d}{2k \cosh \frac{d}{L}} \right) \left(\frac{$$

 $+\frac{J\tau}{1-k2\tau^2}[1-\exp(-Kd)]$

$$= \frac{JtKL}{1 \text{ K}^2L^2} 2 \sinh \frac{d}{2L} \left(\omega \sinh \frac{d}{2L} + \cosh \frac{d}{2L} \right) \frac{(KL-\omega)\exp(-Kd) - (KL+\omega)}{d d d d} + \frac{J\tau}{1-K^2L^2} [1-\exp(-Kd)]$$

$$= \frac{JtKL}{1 \text{ K}^2L^2} 2 \sinh \frac{d}{2L} \left(\omega \sinh \frac{d}{2L} + \cosh \frac{d}{2L} \right) \frac{d}{(\omega^2 \sinh \frac{d}{2L} + 2\omega \cosh + \sinh - 1)} L$$

since
$$\sinh \frac{d}{L} \cosh \frac{d}{2L} = \cosh \frac{d}{L} \sinh \frac{d}{2L} = \cosh \frac{d}{2L}$$

$$\Delta P = \frac{J^{\gamma}KL}{1-K^{2}L^{2}} 2 \sinh \frac{d}{2L} \left(\cosh \frac{d}{2L} + d \sinh \frac{d}{2L} \right) \frac{(KL-d) \exp(-Kd) - (KL+d)}{(d^{2} \sinh \frac{d}{2L} \cosh \frac{d}{2L} + 4 d \sinh \frac{d}{2L} + 2 d + 2 \sinh \frac{d}{2L} \cosh \frac{d}{2L})} + \frac{J^{\gamma}}{1-V^{2}L^{2}} \left[1 - \exp(-Kd) \right]$$

$$\frac{\alpha^{2}2\sinh\frac{d}{2L}\cosh\frac{d}{2L}+4\lambda\sinh^{2}\frac{d}{2L}+2\lambda+2\sinh\frac{d}{2L}\cosh\frac{d}{2L}}{2\sinh\frac{d}{2L}\cosh\frac{d}{2L}}=1+\frac{\alpha^{2}\sinh\frac{d}{2L}\cosh\frac{d}{2L}}{2\ln\frac{d}{2L}\cosh\frac{d}{2L}}$$

$$= 1 + \frac{\lambda^{2} \sinh \frac{d}{2L} \cosh \frac{d}{2L} + \lambda \sinh^{2} \frac{d}{2L} - \lambda \cosh^{2} \frac{d}{2L} + \lambda \cosh^{2} \frac{d}{2L}}{\lambda \sinh^{2} \frac{d}{2L} + \sinh \frac{d}{2L} \cosh \frac{d}{2L}}$$

$$= 1 + \frac{\alpha^{2} \sinh \frac{d}{2L} \cosh \frac{d}{2L}}{\alpha^{2} \sinh^{2} \frac{d}{2L} + \sinh \frac{d}{2L} \cosh \frac{d}{2L}} = 1 + \frac{\alpha^{2} \sinh \frac{d}{2L} (\alpha \sinh \frac{d}{2L} + \cosh \frac{d}{2L})}{(\alpha \sinh \frac{d}{2L} + \cosh \frac{d}{2L})}$$

$$= 1 + 4 \coth \frac{d}{2L}$$

With this, the solution for ΔP reduces to:

$$\Delta P = \frac{Jr}{1-K^2L^2} \left[1 - \exp(-Kd) + KL \frac{(KL-\alpha)\exp(-Kd) - (KL+\alpha)}{1 + \alpha \coth \frac{d}{2L}} \right]$$